Silicon nanoparticles (Si-NPs): Synthesis, Characterization and Application

Thesis submitted to Sikkim University for the partial fulfillment of the degree of Master of Philosophy in Physical Sciences (Physics).

Yanku Lama Sherpa

Roll No: 14MPPY02

Regn. No: 09SU1537

Department of Physical Sciences

School of Physical and Chemical Sciences

SIKKIM UNIVERSITY

Tadong- 737101

Gangtok, Sikkim

2016

सिक्किम विश्वविद्यालय
(भारतीय संसद के अधिनियमद्वारा स्थापित केन्द्रीय विश्वविद्यालय)
गुणवत्तापूर्ण प्रबंधन प्रणाली ISO 9001:2008 हेतु प्रमाणित संस्थान
SIKKIM UNIVERSITY
[A Central University established by an Act of Parliament of India in 2007]
An ISO Quality Management System 9001:2008 Certified Institution

DECLARATION

I declare that the thesis entitled "**Silicon nanoparticles (Si-NPs): synthesis, characterization and application**" submitted by me for the award of **Master of Philosophy (M. Phil.) Degree in Physics** of Sikkim University is my original work. The content of this thesis is based on the experiments which I have performed myself. This thesis has not been submitted for any other degree to any other University.

Date: 20-06-2016

Yanku Iama Sherpa

Roll No: 14MPPY02

Regn. No: 09SU1537

We recommend that the thesis be placed before the Examiners for evaluation.

Supervisor

22/06/16

Dr. Ajay Tripathi

(Assistant Professor)

Department of Physics

Sikkim University

Head

20/6/16

Dr. Amitabha Bhattacharyya

(Associate Professor)

Department of Physics

Sikkim University

Department of Physics
Sikkim University

6 माईल, सामदुर, तादोंग, गंगटोक - 737102 सिक्किम, भारत
दूराभाष : 00-91-3592 - 251067, 251403, फैक्स :- 251067/251757
6th Mile, Samdur, PO Tadong 737102, Gangtok, Sikkim, India
Phones : 00 91 3592 251067, 251403, Fax - 251067/251757
website : www.sikkimuniversity.in/www.sikkimuniversity.ac.in

सिक्किम विश्वविद्यालय
(भारतीय संसद के अधिनियम द्वारा स्थापित केन्द्रीय विश्वविद्यालय)
गुणवत्तापूर्ण प्रबंधन प्रणाली ISO 9001:2008 हेतु प्रमाणित संस्थान
SIKKIM UNIVERSITY
[A Central University established by an Act of Parliament of India in 2007]
An ISO Quality Management System 9001:2008 Certified Institution

Certificate

This is to certify that the thesis entitled "**Silicon nanoparticles (Si-NPs): synthesis, characterization and application**" submitted to Sikkim university in partial fulfillment of the requirements for the degree of **Master of Philosophy (Science) in Physics** embodies the result of *bona fide* research work carried out by **Miss Yanku lama Sherpa** under my guidance and supervision. No part of the thesis has been submitted for any other degree, diploma, associate-ship, fellowship.

All the assistance and help received during the course of the investigation have been duly acknowledged by her.

(Dr. Ajay Tripathi)
M. Phil. Supervisor
Department of physics
School of Physical and Chemical Sciences

Place: Gangtok
Date: 20/06/16

(Dr. Archana Tiwari)
M. Phil. Joint Supervisor
Department of physics
School of Physical and Chemical Sciences

Place: Gangtok
Date: 20/6/2016

6 माईल, सामदुर, तादोंग, गंगटोक - 737102 सिक्किम, भारत
दूराभाष : 00-91-3592 - 251067, 251403, फैक्स :- 251067/251757
6th Mile, Samdur, PO Tadong 737102, Gangtok, Sikkim, India
Phones : 00-91-3592-251067, 251403, Fax - 251067/251757
website : www.sikkimuniversity.in/www.sikkimuniversity.ac.in
Email : sikkimuniversity@gmail.com

Silicon nanoparticles (Si-NPs): Synthesis, Characterization and Application

5th July 2016

0.1 Abstract

The silicon nanoparticles has been extensively investigated after the discovery of visible emission from porous silicon by Canham in 1990s [1]. The size dependent optical property of this material has found its utility not only in optoelectronics but especially in biomedical applications [2, 3, 4, 5, 6]. The semiconductor like CdSe, GaAs etc. based quantum dots have been found to be an ideal candidate in biological imaging but its toxicity towards biological media limits its application in this fields [3, 7, 5]. Due to low biological toxicity [8, 3], high quantum yield [8, 9, 10] and stability in aqueous solution [9, 10] the silicon nanoparticles found to be a good candidate as fluorescent dyes in many biological assays for fluorescence imaging techniques. For this we require synthesis techniques with minimum steps, large scale production and having minimum usage of chemicals. In this work, we report the synthesis of water dispersible silicon nanoparticles by one step procedure using a (3-aminopropyl) trimethoxysilane (APTES), Venyltrimethoxysilane (VTMS) as precursors and ascorbate sodium as a reducing agent. Also we report the plant extract mediated green synthesis of silicon nanoparticles by replacing ascorbate sodium with *Citrus lemon* extract as reducing agent. The synthesis was performed at room temperature and pressure. The synthesized silicon nanoparticles have been characterized using Photoluminescence (PL), UV-Vis spectroscopy, FTIR and Transmission electron microscopy (TEM). These silicon nanoparticles exhibit strong room temperature PL in blue region. The PL in blue region is mainly attributed to the oxide related defects and an attempt has been made to study its optical properties. A compar-

ative study of both the samples prepared from APTES and VTMS using chemical and green reduction techniques have been discussed. The synthesized silicon nanoparticles has been studied as an antimicrobial agent. Also, we checked the feasibility of silicon nanoparticles as fluorescence probe in bio-cell imaging.

Contents

List of Figures

Part I

Introduction

Chapter 1

Introduction

The emergence of nanotechnology has put forward some new application which has changed the lives of the people. This fact stimulates a considerable and detail investigation of nanoparticles as this unlock many potential applications in the field of photonics, catalysis, biomarkers, single photon application, solar cell, UV laser, surface enhanced raman spectroscopy (SERS), chemical and biological sensor [14, 15, 16]. The optical, chemical, mechanical and magnetic properties of nanoparticles as compared to that of its bulk counterparts have led to the revolution especially in the field of biomedical applications [17, 5]. The difference in their property is mainly due to increased surface to volume ratio at nanometer scale [18, 19]. Nanoparticles are basically a bridge between the bulk materials and quantum structure at atomic level. Numerous studies on semiconductor and metal nanoparticles especially silver (Ag) and gold (Au) nanoparticles have been done and detailed investigation have been reported [20]. Semiconductor nanoparticles have received much attention due to their size tunable photoluminescence

(PL) [21]. The size dependent optical properties of semiconductor has been attributed to quantum confinement effect (QCE) [22]. The tunability of emission in semiconductor nanoparticles favours its use in biological imaging as a fluorescence probe. The other advantages are high quantum yield, narrow emission band and high resistance to photobleaching as compared to other organic dyes[10, 5]. Among various types of semiconductor based quantum dots (QDs) such as Cadmium selenide (CdSe), Gallium arsenide (GaAs) have been widely investigated [7, 23, 24]. But their toxicity in biological medium limits their utility towards biomedical application [7]. Silicon nanoparticles (Si-NPs) being abundant and less toxic is found to be potential candidate to replace semiconductor based quantum dots like CdSe, GaAs etc [25, 19, 26]. The discovery of room temperature PL in porous silicon by Canham in 1990s has stimulates a lot of research work for the investigation of the optical properties of Si-NPs [1, 27]. However, it has been identified that the origin of photoluminescence (PL) in Si-NPs are from different sites such as oxide or surface related defect along with quantum confinement effect[8, 9, 28, 22]. Si-NPs are biocompatible due to their smaller size [8, 9, 10] but surface functionalization also enhanced its biocompatibility [8, 9, 10, 29, 26]. Therefore to fabricate the desired Si-NPs, numerous synthesis route were developed as reported in the literature [30, 9, 10]. The well established synthesis routes are electrochemical etching, chemical vapor deposition, laser driven pyrolysis of silane, gas phase synthesis, wet chemistry techniques etc [8, 9, 10, 31, 32, 33, 34, 35, 2, 25]. These synthesis techniques produced hydrophobic Si-NPs which limits their usage in biological application [8, 10]. For biological application, the synthesis of nanoparticles involves

multiple steps such as synthesis, shell growth and surface functionalization [11]. In this work we made an attempt to produce Si-NPs from simpler one step synthesis route. The Si-NPs synthesized from this route are found to have high quantum yield, water dispersible and biocompatible.

1.1 Objectives

So far different methods of synthesis have been reported including ultrasonic dispersion of electrochemically etched silicon, laser-driven pyrolysis of silane, gas phase synthesis, micro emulsion synthesis, wet chemical process, sol gel method etc. which were found complicated which includes firstly synthesis of, secondly coating and thirdly surface functionalization but the method used for the study would be one of the novel method for synthesizing water dispersible silicon nanoparticles with a simple one step procedure using a mild reagents 3-aminopropyl trimethoxysilane (APTES) and ascorbate sodium (AS). The objectives are summerized below

1. Here we try to reproduce the work proposed by Jing et.al. The Si-NPs can be synthesized using the same synthesis protocol and will also perform the synthesis of different samples of Si-NPs using different silane precursor and reducing agents.

2. The synthesized nanoparticles produced from different reagents are characterized by different spectroscopic techniques like UV-Vis spectroscopy, photoluminescence, FTIR and TEM as these techniques are essential to study mainly its optical, electrical and morphological characteristics.

3. To see the effect of changing the precursor in the above proposed synthesis

method.

4. Comparing the above synthesized nanoparticles by adopting the green synthesis method.

5. To see the potential of Synthesized nanoparticles as an antimicrobial agents.

6. Also, the effort will be made on seeing the nanoparticles as a fluorescence probe in cell imaging.

1.2 Outline

The research work presented in this thesis gives a quick and reliable technique for the synthesis of silicon nanoparticles using both chemical and green synthesis route. The structure of thesis is as follows:

Chapter 1 gives brief introduction of Si-NPs and various synthesis techniques for the preparation of Si-NPs. It briefly describe the history of development of Si-NPs where its studies and practical utility has grows exponentially. It briefly explain the unusual physical and optical properties of Si-NPs which has been drastically changed due to the quantum confinement effect and defect centres. It highlighted their usefulness in the field of biomedical applications. It also present objectives and brief outline of thesis.

Chapter 2 gives a detailed insight of semiconductor nanoparticles which outlines the development in the research work done so far in this field. The unusual optical properties of Si-NPs has been explain on the basis of its

bandgap and try to explain the ambiguities in the emission process. It gives some of the features of chemical and green reduction techniques employed for the fabrication of Si-NPs. The current significance of Si-NPs in the context of medical application such as antimicrobial agents and a promising fluorescence probe in biological imaging has been discussed.

Chapter 3 gives the details of materials and method used for synthesis of Si-NPs. The characterization of Si-NPs has been performed using the experimental instrument which has been explain in the context of Si-NPs. In addition the materials and method employed for performing the antimicrobial activity and cell imaging has been given.

Chapter 4 describe the details of results obtained for APTES and VTMS silicon nanoparticles samples i.e. AA and AL. The time dependent studies has been discussed in this chapter. A comparative approach between two sets of samples has been done.

Chapter 5 discussed the application of Si-NPs as fluorescence probe and antimicrobial agents in biomedical applications.

Chapter 6 summarised the whole thesis and also briefly discussed the future prospects of Si-NPs.

Part II

Literature Review

Chapter 2

Literature Review

2.1 Introduction

The new discovered properties of nanoparticles has pave the way for its detail investigation in biological and medical applications. The fluorescence imaging techniques is one such area where the study of nanoparticles have found its profound significance in the last two decades. Fluorescence imaging techniques utilize photoexcited fluorophores whose emission can be detected [3]. The conventional fluorescent dyes like organic dye and fluorescent protein posses serious problem because of broad emission profile thus limiting its usage in this fields [3, 4, 11]. Apart from that photostability is also an issue [4, 3]. Because of this shortcoming of this conventional dyes a growing demand of more robust, sensitive and photostable materials are required [36]. Semiconductor quantum dots has emerged as new class of fluorescent dyes in bioimaging due to its various characteristics properties which are summarised below [5, 3, 37, 24].

1. A narrow emission spectrum reduces spectral overlap which can be set to allows labelling and observation of detailed biological process [38, 3].

2. It offer broad absorption spectra which facilitates the emission of different colors of QDs upon the use of single excitation wavelength [3, 11, 4, 39].

3. The large Stokes shift helps in collection of whole emission spectrum resulting in improved sensitivity of detection [3, 11, 4].

4. QDs provide an efficient platform for drug delivery where it can be incorporated with antibodies to diagnosis and treatment of cancer [38, 30, 26].

5. Photobleaching in organic dyes has found to be eliminated in semiconductor quantum dots [3, 24].

But the toxicity of semiconductor QDs is still an issue. QDs synthesis for bio-

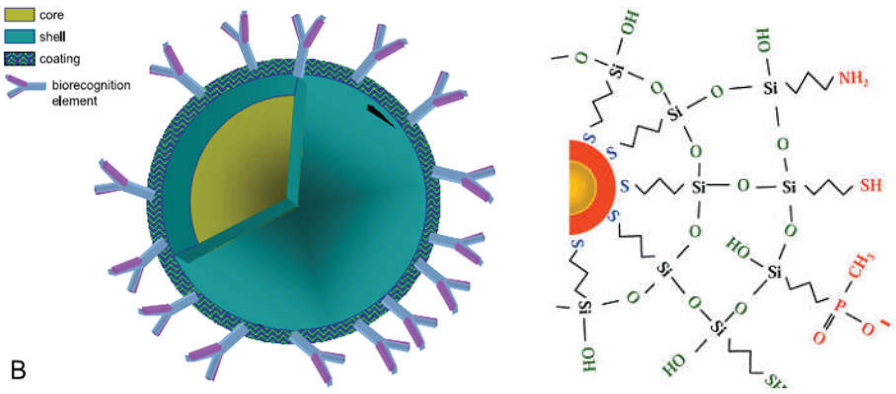

Figure 2.1: Four basic step for QDs synthesis for biological applications [11].

logical application has four basic steps: core synthesis, shell growth, aqueous solubilization and biomolecular conjugation [11]. QDs cores are composed of semiconductor of groups II-VI (CdSe, CdS, CdTe), group IV-VI (PbS, PbSe, PbTe, SnTe) and group III- V (InP) [11]. The performance of Semiconductor QDs as fluorescence probe get enhanced by the surface modification of the

core with organic ligands [40, 3]. To render semiconductor QDs aqueous solubility, coating with hydrophilic polymer like Thiolate ligands(carboxylic acid, amine) or silica is necessary [11, 41, 24]. Thiolate ligands coated Si-NPs found to have better quantum yield and photostability along with narrow emission profile. In particular the QDs functionalized with amine-terminal ligand showed less toxicity than other ligands [11]. The terminal ligand like polyethyline glycol (PEG) QDs showed low level of toxicity but also diminished uptake by cells [11]. The biomolecular conjugation is the crucial step towards checking its applicability in biological imaging [5]. Covalent attachments of biomolcules to QDs is achieved through direct linkages or via small molecule cross linkers. But the QDs coated with silica or silane derivatives during synthesis include functional groups (thiolate ligands) which automatically impart direct conjugation. Most of the core-shell structure like CdSe-ZnS nanoparticles have been investigated for this application [31]. The surface oxidation of CdSe quantum dots release the free radical Cd^{2+} leading to its toxic behavior [3, 7, 5] but capping with ZnS particles found to exhibit less toxicity [7]. The semiconductor QDs is incompatible with polar solvents and have limited utility in biological application.But this multilayered synthesis approach has two limitation. First, it was found to have larger size than standard organic dyes [11] and the second is the optical properties originating from this materials is the consequence of its complex structure [31, 7, 3, 11]. Not only its toxicity but its complex nature inhibits its usage as a probe in bioimaging application. In addition, orange-red emitting labels are desirable [24, 7] since these wavelength are not strongly absorbed by cells and the cells themselves fluoresces at shorter wavelength [3].

2.2 Silicon nanoparticles

Silicon nanoparticles (Si-NPs) are important nanomaterials both for opto-electronics as well as model system for the study of quantum confinement effect (QCE)[42]. The poor light emitting Silicon had seen major setback in many application due to its indirect nature of bangap. The report of visible red luminescence from silicon quantum wire synthesized by electrochemical dissolution of wafers by Canham in 1990s [1] revolutionised it applicability. He attributed the PL origin to two dimensional quantum size effect. This created tremendous studies through investigation about the optical properties of Si-NPs. Wolkin et.al. (1999) [43] prepared porous Si quantum dot samples by electrochemical etching and concluded that the PL of Si quantum dots can be tuned when the surface was passivated with Si-hydrogen (Si-H) bonds. The Si-NPs prepared from thermal evaporation by Chen et. al. (2001) [35] suggested that the PL in particle larger than 9nm is due to surface state induced defects while PL for smaller particle is from quantum confinement effect. Ledoux et. al. (2002) [44] also gives the similar interpretation for smaller particles size of 2nm and 8nm produced by pulsed CO_2 laser pyrolysis of silane. The morphology and different functional groups based optical properties was performed simultaneously and serially by Makino. et.al (2003) [33], Zhu et.al.(2005) [45], Rogozhina et.al(2006) [46], Eckhoff et.al.(2005) [31], Hyun et.al.(2007) [47], Nelles et.al.(2009), Dorofeev et.al.(2009), Eckhoff et.al.(2005) etc. and considerable work was done in this field. Cedrik et.al.(2007) [48] synthesized Si-NPs in gas phase and conducted a study whether the SI-NPs is a direct or indirect bandgap. They concluded

that the Si-NPs has indirect bandgap and the optical properties can also be shown by the indirect bandgap. Parallel studies of Si-NPs in optoelectronics as well as in biomedical application were investigated. The red or orange emission was observed from luminescent colloidal Si-NPs by pyrolysis of silane (Fojtik et.al, 1994)[49]. Their studies bring to light the luminescence quenching phenomena in different solvents. They showed that the quenching was observed in polar solvents (alcohol, ether, chloroform) but mixing with non polar solvents (cyclohexane, CCl_4) does not show any quenching. Similar studies was performed in low polar solvents by Ryabchikov et.al. (2013) [15], where efficient dispersion and excellent stability was achieved [50]. Nirmal et.al. (1999) conducted an experiment both on Si-NPs and CdSe and both materials found to have high quantum yield only if the surface chemistry can be controlled. But the surface chemistry and trapping dynamics in Si-NPs was not understood or uncontrollable. This results encourages further research to achieve better or perhaps ideal fluorophores.

2.3 Electronic structure of silicon nanoparticles

The bandgap between valence band and conduction band is of the fundamental importance to understand the properties of solids. Any change in the gap may significantly alter its physical and optical properties. The bandgap for semiconductor QDs is usually describe by an extended effective mass approximation model (EMA). EMA model demonstrate size dependence of energy level in nanoparticles by assuming particle in a square well potential. In this model, the motion of electron and hole is confide in one or more direction

by potential barriers. Based on the confinement direction, a quantum confide structure are classified into three categories (a) quantum well, (b) quantum wire and (c) quantum dots or nanocrystals. Semiconductor material are

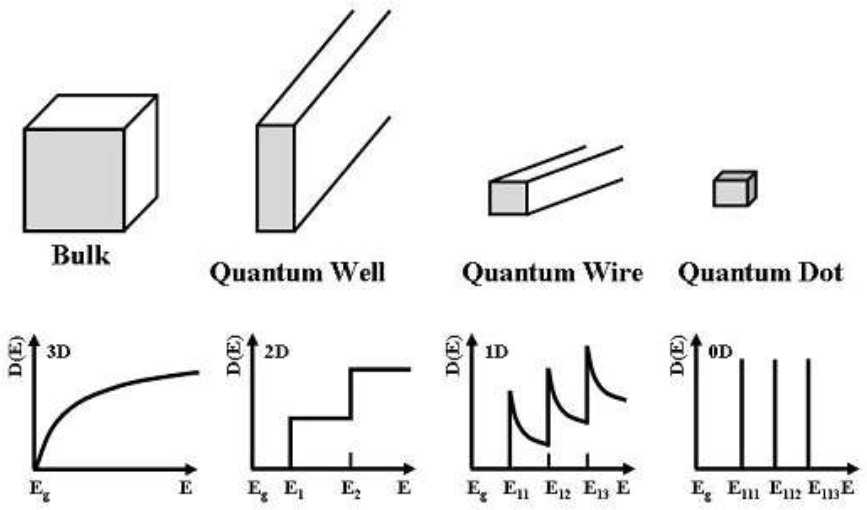

Figure 2.2: A schematic diagram showing density of states (DOS) as a function of the energy for four different types of structures viz. bulk, quantum well, quantum wire and quantum dots [12].

classified into two types on the basis of its energy bandgap in the energy-momentum space as direct and indirect bandgap. In direct bandgap, the transition between valence and conduction band took place between the state with same k-values thereby conserving momentum. But semiconductor with indirect bandgap, the momentum is conserved via the interaction between the phonon and the system. The transition in indirect bandgap is of two step event therefore the optical excitation has very low probabilities. In indirect bandgap the valence band (maximum) and the conduction band (minimum) are misaligned with respect to each other. Hence, the efficiency factor of dir-

ect bandgap is much more than that of the indirect bandgap semiconductor. Bulk silicon has indirect bandgap with no optical property. The empirical

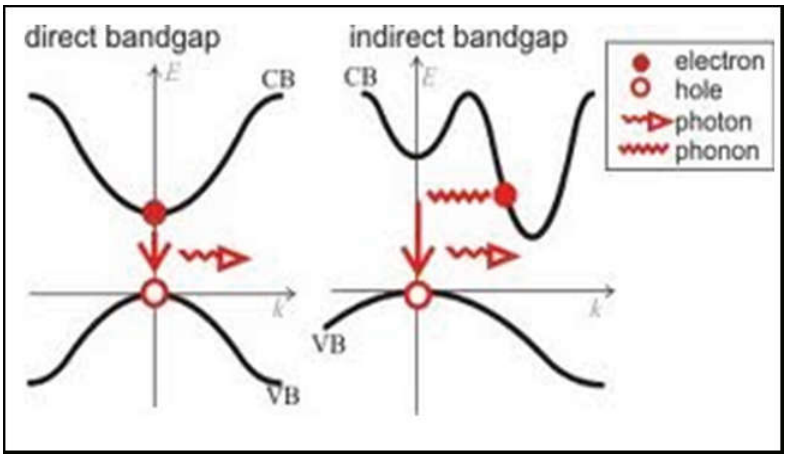

Figure 2.3: Direct and indirect bandgap [13]

relation between a size and electronic bandgap of Si-NPs based on PL results and simulation using linear combination of atomic orbitals (LCAO) has been suggested by Delerue et. al [2, 48, 42].

$$E_g = E_0 + \frac{a}{d^b} \tag{2.1}$$

Where E_g is the Si-NPs bandgap, E_0 is the bandgap of bulk silicon and a and b are parameters which depends on morphology of Si-NPs and d corresponds to the size. This relation is valid for small ($\leq$10nm).For this a and b are calculated to be 3.73 and 1.39 respectively [2, 48, 42]. The spectral shifts observed in porous silicon and later for Si-NPs, suggests that the size dependent optical properties are also present in indirect bandgap semiconductors which has been confirmed from spectral and ellipsometric studies [16]. Semiconductor nanoparticles and clusters are optically active even though its

bulk materials are not [38]. This is because the energy bandgap and phonon distribution is entirely different for nanoparticles than for crystalline bulk. Nanoparticles have localized states which are not present in bulk materials. The transition between this localized may or may not be radiative. Yet they found a profound effect on the actual efficiency of the radiative transition.

2.3.1 Chemical synthesis

To find its application in biological utility, it is imperative to have complete understanding about the optical properties of nanoparticlesi as smaller the particle size, high the surface to volume ratio which is suitable for surface modification. To use Si-NPs practically, the modification of their surface with some functionalized molecules or ligands is essential. The functionalization of Si-NPs with different ligands especially with organic molecules in order to prevent it from agglomerations has been reported using different techniques [21, 32].But however manipulation of surface of Si-NPs ultimately changes the observed optical properties. Therefore chemical route provide the surface modification and till date its a desirable techniques for the Si-NPs fabrication. The amount of chemical utilization in this process is comparably more leaving with some toxic byproduct.

2.3.2 Green synthesis

While most of the chemical synthetic routes are at least two-step methods involving core synthesis and surface-capping steps, but laser ablation of Si-NPs in different liquid environment have received much attention as an effective

and simple one step technique for producing nanoparticles [51, 42, 2]. This technique will render luminescent surface capped Si-NPs as a consequence of ablating in the desired solvent. The fabrication of Si-NPs with tuning of particle size is the main advantages associated with this technique [52, 53]. Vacuum deposition techniques generally involve high temperatures producing nanoparticles in small amount [3]. But this kind of techniques produces Si-NPs suitable for physical and electronic applications. Therefore the study of Si-NPs usable in biological application with this techniques found to have restriction.

Some of the chemical and green synthesis techniques are listed in Table 2.1.

2.4 Silicon nanoparticles as a fluorescence probe in biological imaging

Si-NPs in range 1-100nm recently being exploited as a potential fluorescence probe for diagnostics purposes [37, 8, 9, 10]. The Si-NPs are expected to become new class of fluorescence probe for many biological applications [8, 9, 55]. The surface functionalization can play a major role in interaction with the biological system which defines whether it is biocompatible in nature or not. Previous studies has been done on the alkylated Si-QDs which are hydrophobic [10, 15] and are not soluble. But the recent development in this kind of studies has render them soluble in water which has increase the utilization of Si-NPs in biological imaging. Warner et.al.(2005) [41] crafted a room temperature water soluble silicon QDs using hydride as a reducing

agents that exhibit strong blue PL with rapid rate of recombination. The silicon QDs modified by allylamine showed better photobleaching stability than rhodamine 6G in water and demonstrated the suitability of this Silicon QDs as chromophore in biological imaging performed in cytosol of HeLa cells. Wang et.al.(2009) [10] report a synthesis of acrylic acid-grafted water dispersible Si-NPs by electrochemical etching with hydrofluoric acid (HF). The novel features of this fabrication is that they obtained strong red PL at room temperature which is the major requirement in the biological imaging. Following the same, Manhat et.al(2011) synthesized glutaric acid-grafted Si-NPs which exhibit blue green emission with short fluorescence lifetime (ns) [9]. Wang et.al(2014) [8] presented his paper with the first report of green synthesis of Si-NPs on large scale and at low cost. They synthesis Si-NPs with a simple one step procedure using APTES as a precursor and ascorbate sodium as a reducing agent. The Si-NPs prepared from this method are water dispersible and hydrophilic (prevents aggregation) due to the kind of functionalized groups present in it. They demonstrated the effective imaging of Si-NPs with the fluorescence lifetime imaging microscope (FLIM) techniques which suppressed the autofluorescence of cellular fluorophores. Thus making it promising probes for cell imaging. The most important features of Si-NPs is that it does not show any morphological damage to the cell upon staining which is the greatest achievement in the biological application [10, 30].

2.5 Silicon nanoparticles as an antimicrobial agents

Recently it has been found that the certain strain of bacteria has developed a resistance against common antibiotics which has led to find the novel strategies for the treatment of infections associated to antimicrobial resistance in affected patients [56, 29]. Due to high thermal and chemical stability, high surface area and good biocompatibility, silica nanoparticles are a good option to deliver drugs such as antibiotics [56]. It has been demonstrated recently that highly reactive metal oxide nanoparticles exhibit excellent efficacy against gram positive bacteria and gram negative bacteria [29]. The biocidal effects of copper and silver nanoparticles have been widely reported [56]. They are very effective in reducing the microbial density in vitro, but their cytotoxicity towards mammalian cells has also been found to be high. Therefore the incorporation of silver and copper into silica nanoparticles has allow the reduction of concentration of metal ions needed to achieve antimicrobial activity [57]. The antimicrobial performance of silica nanoparticles have been greatly improved with the functionalization of N-halamine polymer with core shell nanoparticles which displayed better efficacy against gram positive bacteria and gram negative bacteria [58]. The mesoporous silica nanospheres modified with nanocrystalline titanium dioxide were successfully fabricated and used as a photoactivated antibacterial agent. Nitric oxide releasing silica nanoparticles which has been prepared from N-Methylaminopropyltrimethoxysilane (MAP3) and N-(6-inohexyl) aminopropyltrimethoxysilane (AHAP3) have shown its efficacy

against the microorganisms such as *Pseudomonas aeruginosa* and *Escherichia coli* [59]. The MAP3 silica nanoparticles had 1000-fold greater efficacy against *P. aeruginosa* than the AHAP3 nanoparticles due to the smaller size of MAP3 nanoparticles that allow them to penetrate biofilm matrix more effectively [59].

Table 2.1: Overview of synthesis of Si-NPs by chemical and green reduction techniques

Chemical synthesis	Protocol for synthesis	NPs size	References
Wet chemistry	Reduction of silicon tetrachloride($SiCl_3$) with sodium napthalide	∼4nm	[32]
Electrochemical etching	Porous silicon obtained by electrochemical etching with HF	∼5nm ∼1nm	[10] [31]
Sol gel techniques	It involves the centrifuge assisted size-selective deposition of NPs from a colloidal solution (sol) containing nc-Si powders.	10-100nm	[54]
Green synthesis	Features		
Laser ablation in gaseous phase	Ablation of silicon H_2 target in and Ar gas	∼5nm 1-10nm 2.5 and 8nm	[33] [34] [44]
Laser ablation in liquid media	Ablation of silicon wafer in different solvent.	∼20nm(5-200nm) 2-5nm	[42] [51]
Vapour deposition	Thermal evaporation of silicon chip	3-50nm ∼20nm	[35] [45]
Spark discharge	Electrical spark discharge between two plane silicon electrodes immersed) in deionized water(DI)	3-8nm 3-5nm	[2] [25]

Part III

Materials and Method

Chapter 3

Materials and Method

We investigate Si-NPs prepared from one step procedure where the synthesis protocol have been adopted from Wang et al [8]. The samples were synthesized with two different techniques i.e. chemical and green reduction techniques.

3.1 Chemical reagents

3-aminopropyltrimethoxysilane (APTES 97%) and Venyltrimethoxysilane (VTMS 98%) were purchased from Sigma Aldrich. The Ascorbate sodium (AS 99-101.0%) was purchased from Loba Chemie. *Citrus Lemon* was purchased from local shop. The glassware were thoroughly washed, cleaned with ethanol/acetone and rinsed thoroughly with deionised water. The materials required for the synthesis of Si-NPs are given in detail in Table 3.1.

Table 3.1: Materials required for the synthesis of silicon nanoparticles.

Sample	Precursor	Reducing agents
APTES AS(AA)	Aminopropyl trimethoxysilane (APTES)	Ascorbate sodium(AS)
APTES CITRUS LEMON(AL)	Aminopropyl trimethoxysilane (APTES)	Lemon (Ascorbic acid)
VTMS AS (VA)	Venyltri-methoxysilane (VTMS)	Ascorbate Sodium(AS)
VTMS CITRUS LEMON (VL)	Venyltri-methoxysilane (VTMS)	Lemon (Ascorbic acid)

3.2 Preparation of silicon nanoparticles

The synthesis were carried out by adding 1mL of aminopropyltrimethoxysilane (APTES) to 4mL of aqueous solution. Then 1.25mL of 0.1M ascorbate sodium (AS) was added. After this the solution was stirred for 25 minutes in magnetic stirrer (700 rpm). The whole procedure was completed in 35 minutes. Now the second synthesis was carried out using the same protocol

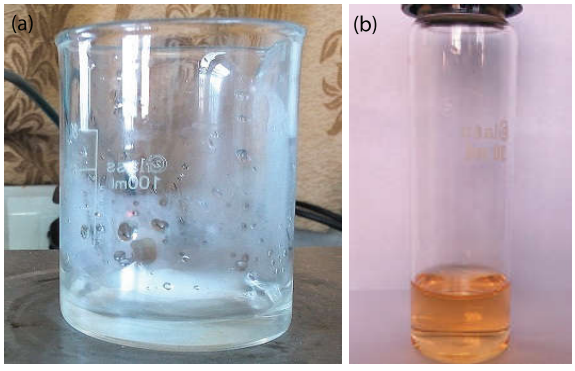

Figure 3.1: Synthesis of Si-NPs using APTES and ascorbate sodium.

as above by just substituting the silane materials with venyltrimethoxysialne (VTMS) instead of aminopropyltrimethoxysilane (APTES). The green reduction techniques was actualized using an extract from *Citrus lemon* which act as a reducing agents and using same silane materials as above. Altogether, we have synthesized four different Si-NPs namely: Aptes + AS (AA), APTES + *Citrus lemon* (AL), VTMS + AS (VA) and VTMS +*Citrus lemon* (VL). The synthesized Si-NPs were confirmed by observing them under uv irradiation.

Figure 3.2: Si-NPs under uv irradiation.

3.3 Characterization of silicon nanoparticles

3.3.1 UV-Vis absorption spectroscopy

In absorption spectroscopy, the process of absorption of energy required for the transition from lower energy state to higher energy state is exactly equivalent to the energy of electromagnetic radiation that causes the transition. The absorbtion spectrum contain all possible transition [60]. UV-Vis spectroscopy studies the changes in electronic energy levels within the molecule arising due to transfer of electrons from π or non-bonding orbitals to an-

tibonding orbitals. The absorption spectroscopy was performed using a Perkin Elmer made Lambda 750 spectrophotometer which was equipped with Deuterium and Tungsten lamps as the light source emitting in the range of 190nm to 380nm and 380nm to 800nm respectively.

3.3.2 Photoluminescence

Photoluminescence is by far the most widely used optical characterization method in Si-NPs investigations. For this technique, light of sufficient energy is incident on a material which creates electrons and holes [27]. These excess carriers subsequently recombine radiatively and some of them non radiatively. In the case of radiative emission, the emitted light is called PL. This light can be collected and analyzed to obtained the information about the photoexcited material. The PL spectrum provides the transition energies, which can be used to determine electronic energy levels. The PL intensity gives a measure of the relative rates of radiative and nonradiative recombination. The PL depends on the optical excitation. The PL spectra of bulk semiconductor is rather impossible as they have indirect bandgap but however dangling bonds at a semiconductor nanoparticles surface or interface give rise to electronic states within the bandgap. The PL measurement in our samples were recorded in Perkin Elmer LS55 fluorescence spectroscopy with 300nm-400nm applied excitation wavelength and the emission were recorded between 320nm-800nm.

3.3.3 Fourier transform infrared spectroscopy

To examine the nature of the Si-NPs surface more closely, Perkin Elmer FTIR spectroscopy was used in the scanning range from 700 $cm^{-}1$ to $4000cm^{-}1$. An infrared spectrum is a fingerprint of a materials. Because each different materials is a unique combination of atoms, no two compounds can have exact same infrared spectrum. Therefore infrared spectroscopy gives a positive identification (qualitative analysis) of every different kind of materials. The total internal energy of a molecule are the sum of rotational, vibrational and electronic energy levels. Infrared spectroscopy is the study of interactions between matter and electromagnetic fields in the IR region based on the molecular vibration. The molecule are excited to higher vibrational state by absorbing IR radiation. In general, a frequency is strongly absorbed if its photons energy matches with the vibrational energy levels of the molecule. The original infrared spectroscopy is of dispersive type and fourier transform infrared spectroscopy (FTIR) was developed in order to overcome the limitation encountered with dispersive instruments. The main difficulty was the slow scanning process. A method for measuring all of the infrared frequencies simultaneously, rather than individually, was needed which employed an optical device called an interferometer in place of prism or grating. The use of interferometer results in extremely fast measurements. The measured frequency spectrum cannot be interpreted directly. A means of decoding the individual frequencies are required. This can be accomplished with a well-known mathematical technique called the Fourier transformation and

its mathematical expression can be written as

$$F(\omega) = \int_{-\infty}^{\infty} f(x) e^{i\omega t} \tag{3.1}$$

and the reverse fourier transform is

$$F(\omega) = \frac{1}{2\pi} \int_{-\infty}^{\infty} f(x) e^{i\omega t} \tag{3.2}$$

where ω is an angular frequency and x is the optical path difference in our case. F(ω) is the spectrum and f(x) is called the interferogram.

3.3.4 Transmission electron microscopy

The TEM technique has been used to provide the detailed information on the internal structure of Si-NPs. The images of Si-NPs were obtained with resolution upto atomic scale. To apply this method of analysis, a high energy beam of electrons is fired in vacuum through a thin, electron-transparent region of the sample of interest. An image of the sample is impressed into the transmitted electron beam and is magnified by subsequent electromagnetic lenses. The image, with a magnification of up to or beyond a million times, is finally displayed on a fluorescent screen for recording on photographic film or on a TV monitor using an appropriate pick-up system [27]. TEM images were obtained using technai equipped with thermo-ionic electron gun working at 200 kV.

Table 3.2: Media and test pathogens

Media	Test pathogens		
	Gram positive bacteria	Gram negative bacteria	Fungi
NA	*Bacillus subtilis* MTCC 441	*Escherichia coli* MTCC 739	*Candida albicans* MTCC 227
PDA	*Bacillus subtilis* MTCC 2757	*Escherichia coli* MTCC 10312	*Trichophyto rubrum* ANTR01

3.4 Antimicrobial studies using disc diffusion method

The antimicrobial experiment was performed in the Regional Research Centre of Biotechnology, Tadong, under the supervision of Dr. L. S. Singh. The antimicrobial susceptibility testing was carried using the disc diffusion method according to standard method to assess the presence of antimicrobial activities of the silicon nanoparticles. The details of the media and test organism used are given in Table 3.2.

Nutrient agar (NA) and Potato Dextrose Agar (PDA) from HiMedia, Mumbai were used to study the antimicrobial properties of the silicon nanoparticles.Bacterial and fungal pathogens were used for screening the antimicrobial efficacy of the test samples. Bacterial strains viz. *Escherichia coli* MTCC 739, *Escherichia coli* MTCC 10312, *Bacillus subtilis* MTCC 441, *Bacillus subtilis* MTCC 2757 and fungal strains viz. *Candida albicans* MTCC 227 and *Trichophyton rubrum* ANTR01.

Bacterial and fungal suspension with 1x10^8 cfu/mL and 3.15x10^7 cfu/mL respectively were used to lawn NA and PDA plates evenly using sterile swabs. The plates were dried for 15 minutes and then used for the sensitivity test.The discs which had been impregnated with a series of silicon nanoparticles were placed on the NA and PDA surface.Each test plate comprised of two discs where one was negative control and other was a treated disc. sterile water was used as a negative control.The plates were then incubated at 37°C and 28°C for bacterial and fungal cultures respectively for 24 to 48 hours.After the incubation, the plates were examined for inhibition zone.The diameter of inhibition zone were measured and recorded.The minimum inhibition concentrations (MICs) was determined using Inhibitory concentration in Diffusion (ICD) method. It is done by carrying out the diffusion test with three discs of different concentration of silicon nanoparticles similar to the concentration used in the sensitivity tests against bacterial and fungal cultures. The lowest concentration of sample that inhibits the growth of test organisms was considered as the MIC value for each of the bacterial and fungal organism.

3.5 Biological imaging of living cell

3.5.1 Cell treatment and imaging experiment

The cell imaging experiment using fluorescence microscopy was performed under the supervision of Dr. Amlan Gupta, Sikkim manipal institute of medical sciences (SMIMS). The human white blood cells (WBCs) were provided by the Department of pathology, (SMIMS). The fluorescence imaging of hu-

man WBCs were performed with two different concentration of Si-NPs viz. $6.16\,\mu g\,ml^{-1}$ and $1.54\,\mu g\,ml^{-1}$. The cells were seeded in dishes containing DMEM medium and from each concentration a 50microlitre per mL was added to dishes and incubated in a fully humidified incubator at 37°C with 5% CO_2 for 1.5 h. After the incubation the cell were ready for imaging measurements. The fluorescence images of cellular Si-NPs were acquired with a fluorescence inverted microscope with leica DFC camera (make-leica), model-Dmil led fluo with 50 W Hg and 100W Hg as a light source.

Part IV

Results and Discussion

Chapter 4

Chemical and Green synthesis using APTES.

In this thesis Si-NPs are synthesized using the techniques adopted by Wang et al [9] where APTES acts as a precursor and ascorbate sodium as a reducing agent. The synthesized Si-NPs are abbreviated as AA and synthesis route is considered as chemical synthesis. In addition we have modified this synthesis route by replacing the reducing agent with *Citrus lemon* extract. The synthesized Si-NPs are abbreviated as AL and this synthesis route is considered as green synthesis. The synthesized Si-NPs have been characterized by using UV-Vis spectroscopy, photoluminescence spectroscopy, FTIR spectroscopy and micrographs TEM. In this chapter the obtained results are discussed for sample AA and AL.

4.1 Spectroscopic characterization of silicon nanoparticles

4.1.1 UV-Vis spectroscopy

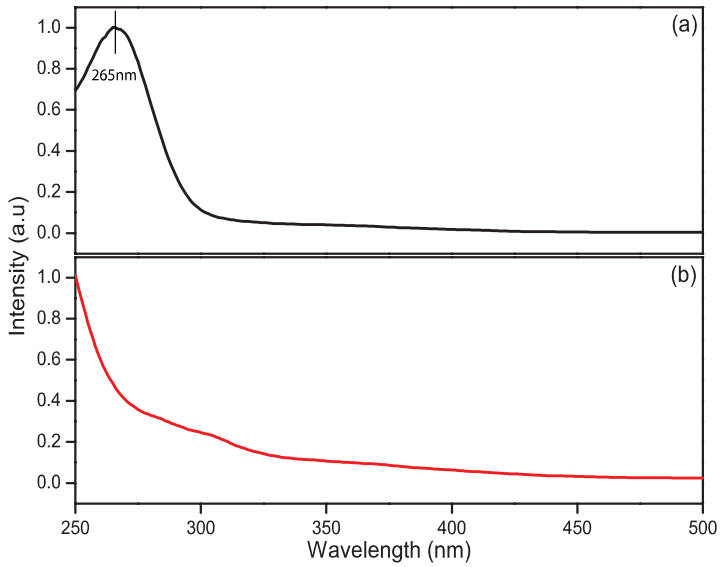

Figure 4.1: UV-Vis spectrum of (a) AA and (b) AL at room temperature in the range from 200nm to 800nm on the freshly prepared samples.

Si-NPs synthesized using the chemical and green route which under the UV irradiation exhibit green fluorescence confirming the synthesis of Si-NPs [8]. These Si-NPs are water dispersible, hydrophilic and stable in aqueous solution . For reference see Figure 3.2 in chapter 3 : Materials and Method . The UV-Vis measurement were done on the freshly prepared samples. Figure 4.1 (a) shows the UV-Vis spectra of (a) AA and and Figure 4.1(b) of AL at room temperature in the range from 200nm to 800nm.

In the sample AA, the spectrum shows a gradual increase in absorption

below 450nm with peak appearing at 265 corresponding to reducing agent i.e. ascorbate sodium. The gradual increase in the absorption at lower wavelength is the characteristics absorption spectrum of Si-NPs [8, 10, 2]. The same trend in the absorption spectrum is being observed in AL. In both cases the absorption tail in the visible region is associated with indirect transitions in bulk silicon [2]. As compared to AA, in AL the band edges is shifted towards lower wavelength. This indicates the Si-NPs in AL are smaller in size as compared to AA. From this we can conclude that *Citrus lemon* is a good reducing agent as compared to ascorbate sodium.

4.1.2 Photoluminescence

As observed from UV-Vis spectra of AA and AL that both samples absorbs the wavelength below 450nm. In addition, an UV irradiation on these Si-NPs also exhibit green fluorescence which can be observed through naked eye. In order to elucidate the PL properties of AA and AL, several excitation wavelength ranging between 300nm to 400nm are used. The same solution used in UV-Vis spectroscopy were subsequently used for the PL measurement.

The PL spectra for AA is shown in Figure 4.2 (a) and for AL in Figure 4.3 (a). For AA, the PL have broad disturbed gaussian profile ranging from 440nm and 495nm. By varying the excitation wavelength no shift is been observed. After 370nm, no contribution in PL is seen from the particle emitting at 440nm. The broad distribution of emission from 400nm to 600nm mainly covers the blue green region. Emission in blue green region may be

attributed to the oxide related defects giving rise to numbers of metastables excitonic levels in between the main absorption band [45, 35, 51, 61, 62]. Along with PL, the photoluminescence excitation spectroscopy (PLE) were

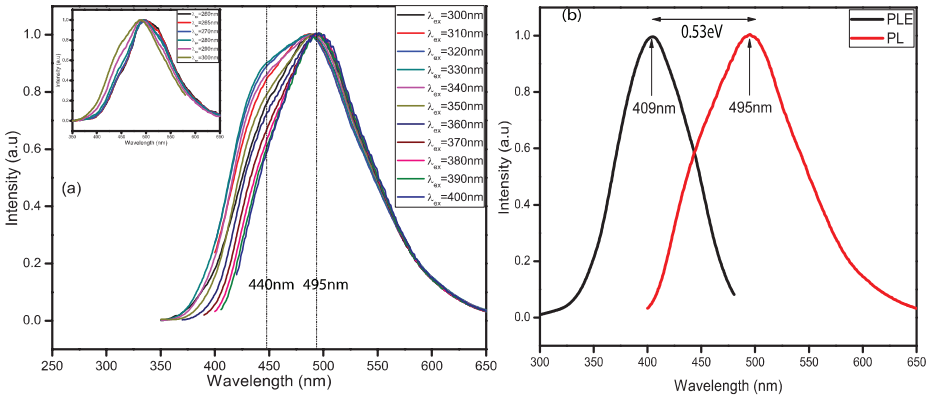

Figure 4.2: (a) PL of AA at room temperature at different excitation wavelength from 300nm to 400nm on the freshly prepared sample, (b) normalized PL and PLE spectra of AA.

also performed to understand the energy level diagram of Si-NPs more precisely. The normalized PL and PLE spectra are shown n Figure 4.2(b). The PLE spectra was recorded while monitoring a fixed emission wavelength at 495nm which is also the most intense peak in PL spectrum of AA. The PLE spectrum shows the absorption peak at 409nm with FWHM of 72nm. The stokes shift between the emission and absorption band is found to be 0.53eV. The existence of stokes shift between PL and PLE indicates that PL in visible region has been originated from the radiative recombination of electron-hole pair from the defect states at the surface of the Si NPs [63]. The smaller particles have very large stokes shift as compared to large particle and stokes shift become zero for infinite particle size [19]. The reduction in size of nanoparticles create disorder and strained bond at the surface and

as consequences we see large stokes shift in smaller particles [63]. Therefore the origin of PL is attributed to oxide related defects which may have arise because of the creation of oxide layers on the surface of Si-NPs due to the reaction between the Si-NPs and water in the solution.

Similarly to AA, we have also performed the PL measurement for AL. In

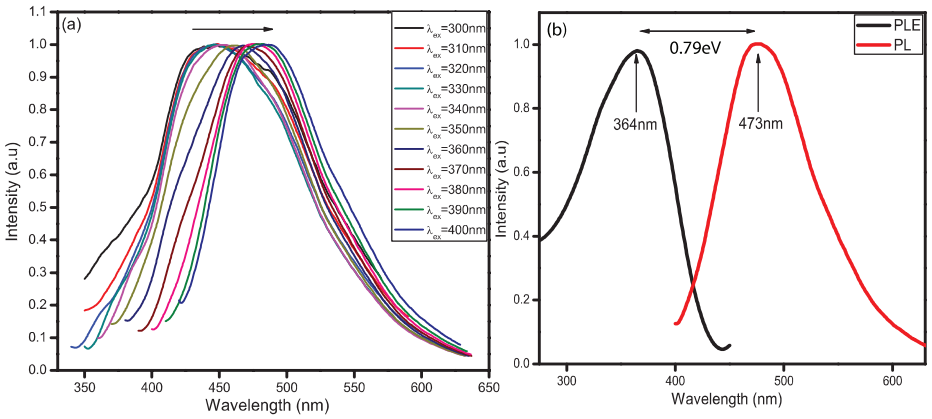

Figure 4.3: (a) PL of AL at room temperature at different excitation wavelength from 300nm to 400nm on the freshly prepared sample, (b) normalized PL and PLE spectra of AL.

AL, PL have been also recorded for excitation wavelength ranging between 300nm to 400nm. The emission profile over all the excitation wavelength shows broad gaussian profile in blue green region. The normalised PL and PLE spectra are shown in Figure 4.3(b). The PLE spectra shows the absorption peak at 364nm with emission wavelength fixed at 473nm. Contrary to AA, the PL spectrum of AL shows that emission shifts from 450nm to 485nm (redshift of 35nm) when the excitation wavelength is varied from 300nm to 400nm. This tunability can be attributed to the inhomogeneity of the size distribution of synthesized Si-NPs. Another possible reason may be the synthesized Si-NPs are not stable in solution and they are all agglomerating

giving rise to large size. The stokes shift between the emission and absorption band is found to be 0.79eV. The stokes shift is large in AL as compared to AA which confirmed the formation of smaller sized nanoparticles in AL.

4.2 Fourier transform infrared spectroscopy

To examine the main chemical bonds present in Si-NPs, the FTIR spectrum was obtained and measured. Figure 4.4 shows the FTIR spectrum of (a) AA and (b) AL on the freshly prepared samples in the scanning range from 700cm^{-1} to 4000cm^{-1}. The sharp absorbance peak at 1018cm^{-1} is ascribed to Si-O-Si bonding in AA and AL [64, 65]. The broad absorbance peak at around 1410cm^{-1} is due to N-H bending vibration[8]. The absorbance in the range from 2870cm^{-1} to 2960cm^{-1} is attributed to O-H bond [8].

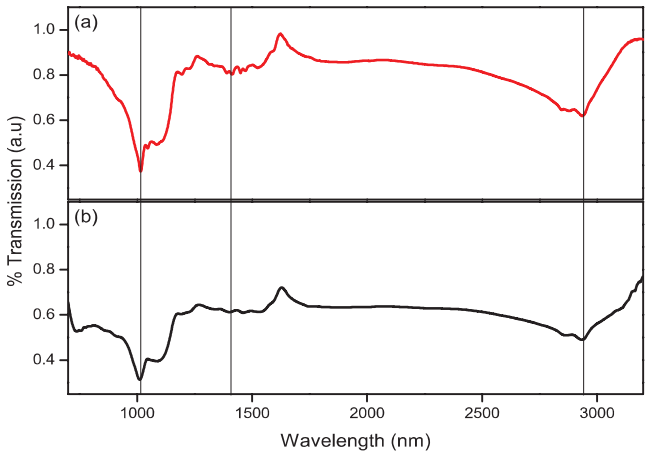

Figure 4.4: FTIR spectrum of (a) AA and (b) AL in the scanning range from 700cm^{-1} to 4000cm^{-1} on the freshly prepared samples.

4.3 Transmission electron microscopy

Transmission electron microscopy (TEM) was performed in the Department of physical sciences, Hyderabad Central University under the supervision of Dr. A. P. Pathak. The measurement were recorded for the month old samples. Figure 4.5 shows the TEM images of (a) AA and (b) AL. It can be seen that the shape of the particles are nearly spherical. The size of the Si-NPs were obtained by using the ImageJ software. The average diameter of particles are found to be 34nm (± 8nm) for AA and 48nm (± 10nm) for AL.

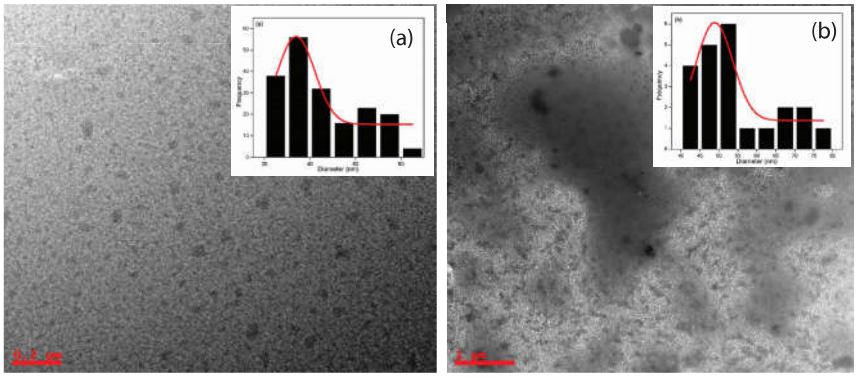

Figure 4.5: Particle sizes analysis histogram of (a) AA and (b) AL calculated from TEM images.

4.4 Ageing effects on the optical properties of silicon nanoparticles

We have studied the optical property of synthesized Si-NPs as function of reduction time in order to check the stability of Si-NPs in aqueous solution.

4.4.1 UV-Vis spectroscopy

The interesting optical properties of Si-NPs may find potential applications in the biological systems. The broad absorption spectrum of Si-NPs is desirable in bioimaging application. The stability of Si-NPs in an aqueous solution over a period of time is important for such applications. Therefore we have performed a time dependent study of the optical properties as a function of reduction time. The absorption data for samples of Si-NPs viz. AA and AL were recorded for two subsequent weeks i.e. on the 1st, 7th and 14th day of synthesis. On the freshly prepared sample of AA, there is a gradual increase

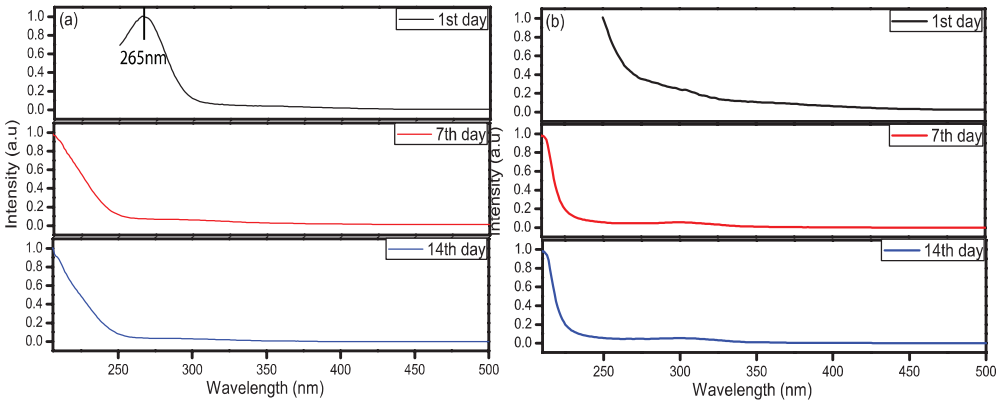

Figure 4.6: UV-Vis spectra of (a) AA and (b) AL on 1st, 7th and 14th day in the scanning range from 200nm to 800nm.

in absorbance at lower wavelength with a peak at 265nm. In the spectra recorded on the 7th and 14th day the peak at 265nm disappears and band edge shifts towards shorter wavelengths. Similar trend is been observed in AL. But contrary to AA no peak has been observed. Like in AA, band edge shifts towards shorter wavelengths. The shift of band edge towards shorter wavelength in both AA and AL with time can be attributed to reduction

of large sized Si-NPs to the smaller size nanoparticles [19]. The blueshift in both the samples of Si-NPs may be attributed to the surface oxidation [66].

4.4.2 Photoluminescence

The lack of PL stability (photostability) of Si-NPs is been the major constraints in their biological applications [4]. To investigate the photostability of Si-NPs in aqueous solution, time dependent PL studies were also performed. For AA and AL, the PL spectra were recorded from 400nm to 600nm using an excitation wavelength of 370nm. The PL spectra for the 1st, 7th and 14th day of synthesized AA are shown in Figure 4.7 (a) and for AL in Figure 4.8 (a). In AA the curve fitting of PL spectra gives two deconvulated peaks P1 (centered at 495nm) and P2 (centered at 440nm). With increasing ageing times the increase in intensity of peak P2 observed. The PL spectra for 1st, 7th and 14th day with two deconvulated peaks are shown in Figure 4.7 (b). On the first day of synthesis, the relative intensity ratio, I_{p1} $/I_{p2}$ comes out to be 2.39. This ratio gradually drops and on 14th day the recorded ratio is found to be 1.67. After 14th day the recorded intensity ratio shows no variation indicating the stable configuration of AA. The PL mechanism in AA using an electronic bandgap is shown in figure 4.7 (c). On the 1st day of synthesis, the particles emitting at longer wavelength (495) having smaller bandgap are maximum with respect to the particles emitting at shorter wavelength (440nm) having larger bandgap which indicates the formation of larger particle. On the 7th day from the synthesis, the intensity of particles emitting at longer wavelength remains more or less same and

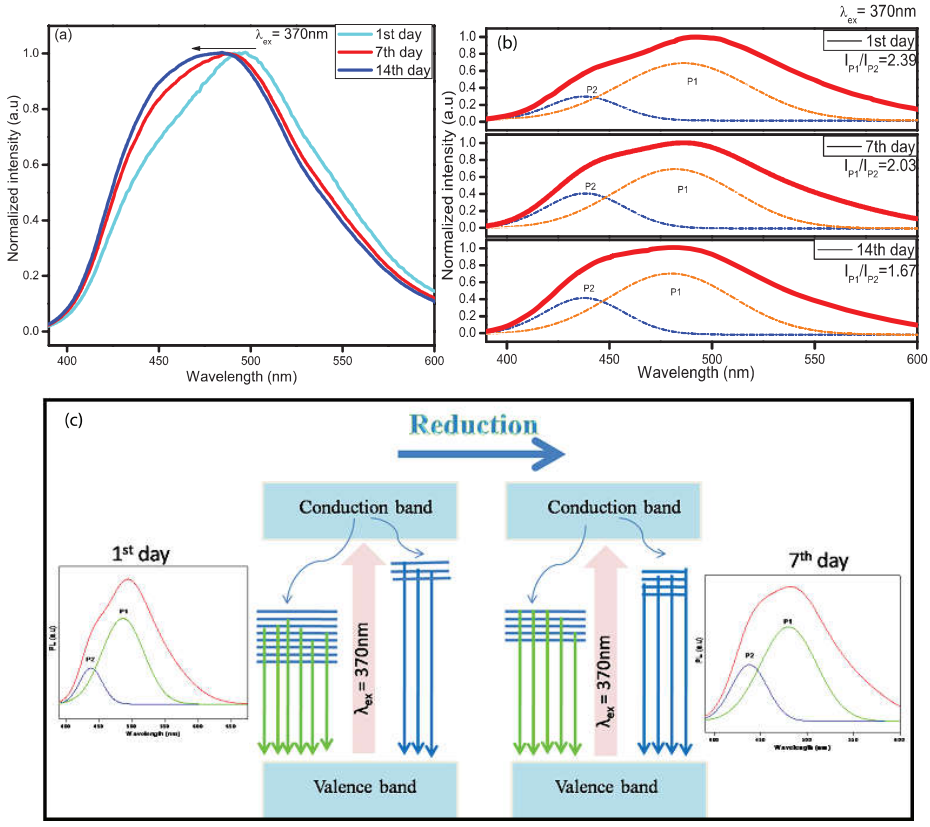

Figure 4.7: PL spectra of (a) AA on 1st, 7th and 14th day in the scanning range from 200nm to 800nm at an excitation wavelength of 370nm, (b) PL spectra of AA with two deconvoluted gaussian band of P1 and P2 as a function of reduction time and orange and blue line are the envelope of deconvulated peaks (c) The proposed PL mechanisms of the predominant P1 emission and P2 emission in AL with green and blue line are the envelope of deconvulated peaks.

particles emitting at shorter wavelength are increasing. This suggest that with ageing, smaller size Si-NPs are getting synthesized along with remaining large sized nanoparticles which explains the small shift towards shorter wavelength in the sample AA.

In AL, the peak centered at 473nm on the 1st day of synthesis has been blueshifted to 450nm on the 7th and 14th day of synthesis. The peak position has been blueshifted by 23nm towards shorter wavelength. The curve fitting of PL spectra shows the presence of two deconvulated peaks having centered at 473nm (P1) and 450nm (P2) are shown in Figure 4.8 (b). On the 1st day of synthesis, the PL is dominated by emission centered at P2 with small contribution from P1. The observed relative intensity ratio I_{p1} $/I_{p2}$ comes out to be 14.4 but with ageing of the solution the ratio drops to 1.22 on the 7th day and remain same on 14th day. There after no change has been observed in the intensity ratio. This results suggest that the reduction process in AL is fast as compared to AA and also completed by 7th day of synthesis. The PL mechanism for this sample have been also explained on the basis of electronic bandgap as shown in Figure 4.8 (c). Here the particles emitting at shorter wavelengths having larger bandgap are very few in number as compared to particles emitting at longer wavelengths having smaller bandgap. This suggest that the larger particles have been synthesized on the first day of synthesis and with reduction, the number of particles emitting from defect centres at longer wavelength are decreasing.

The emission peak of AA and AL at 495nm and 473nm suggest the formation of smaller particles in AL as compared to AA. With ageing, the emission spectra of AA shows negligible shift towards shorter wavelength which indic-

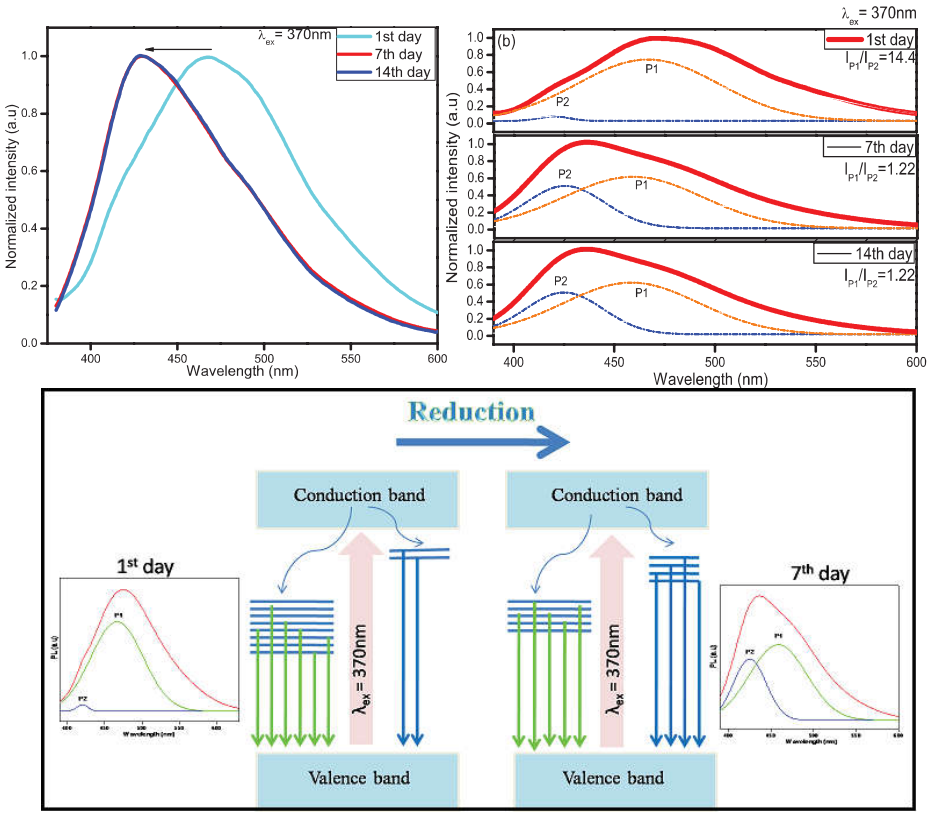

Figure 4.8: PL spectra of (a) AL on 1st, 7th and 14th day in the scanning range from 200nm to 800nm at an excitation wavelength of 370nm, (b) Curve fitting of PL spectra of AL with two deconvoluted gaussian band of P1 and P2 as a function of reduction time and orange and blue line are the envelope of deconvulated peaks (c) The proposed PL mechanisms of the predominant P1 emission and P2 emission in AL with green and blue line are the envelope of deconvulated peaks.

ates the broad distribution of nanoparticles sizes. But contrary to AA, in AL there is a blueshift in emission peak which suggest the formation of even smaller particles with ageing [67]. With ageing, the blueshift in Si-NPs is mainly caused from the reduction in sizes which may be attributed to surface oxidation of sample [35]. The surface oxidation creates metastables states leading to an obvious redshift in the sample spectrum but this same metastable states are also responsible for the blueshift seen in our sample spectrum as well [45, 66, 47]. The sample AA prepared using ascorbate sodium as reducing agent leads to broadening of PL whereas the sample AL prepared from *Citrus lemon* as reducing agent resulted in blueshift. These results suggest that the *Citrus lemon* is a better reducing agent than ascorbate sodium.

4.5 Fourier transform infrared spectroscopy

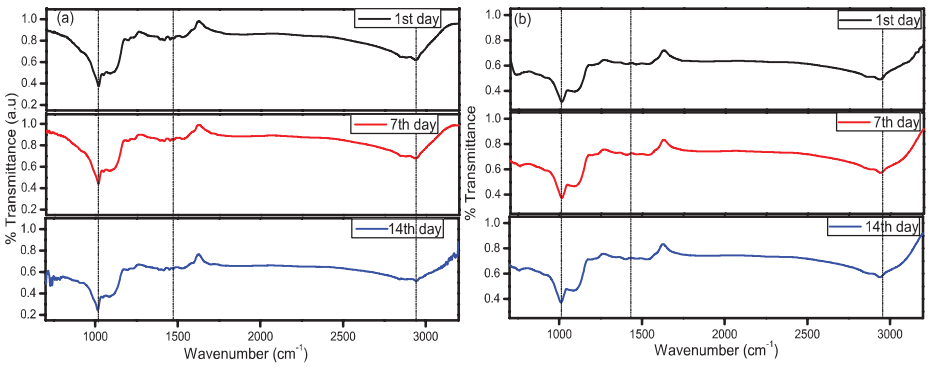

Figure 4.9: FTIR spectra of (a) AA and (b) AL on the 1st, 7th and 14th day in the scanning range from 700cm^{-}1 to 4000cm^{-}1.

To see the changes in the chemical bonding with ageing we also performed a time dependent studies in FTIR spectroscopy. The FTIR spectrum were

obtained for two subsequent weeks. Figure 4.9 shows the time dependent FTIR spectrum of (a) AA and (b) AL on the 1st, 7th and 14th day from 700cm^{-1} to 4000cm^{-1}. The sharp absorbance peak 1018cm^{-1} which was ascribed to Si-O-Si bonding in AA and AL [64] does not change with ageing. The broad absorbance peak at around 1410cm^{-1} due to N-H bending vibration and the absorbance in the range from 2870cm^{-1} to 2960cm^{-1} attributed to O-H bond [8] does not show any change with ageing in both the samples. It suggest that the oxidation is the main reason behind its optical properties but with ageing in both the samples, none of the peak show any changes in the bond.

Chapter 5

Chemical and Green synthesis using VTMS.

In this chapter we have explore the synthesis of Si-NPs using silicon precursor namely VTMS. The synthesis protocol remain the same as before. For chemical synthesis, we have used ascorbate sodium as reducing agent and the Si-NPs prepared using this method is called VA. For green synthesis, we have used *Citrus lemon* as reducing agent and synthesized Si-NPs is abbreviated as VL. The synthesized Si-NPs have been characterized by using UV-Vis spectroscopy, photoluminescence spectroscopy, FTIR spectroscopy and micrographs TEM. In this chapter the obtained results are discussed.

5.1 Spectroscopic characterization of silicon nanoparticles

5.1.1 UV-Vis spectroscopy

The UV-Vis measurement were performed similar to AA and AL. Si-NPs prepared using both chemical and green route were characterized on the freshly prepared samples. The sample solution exhibit green fluorescence under UV irradiation which confirms the synthesis of Si-NPs. These Si-NPs are water dispersible, hydrophilic and stable in aqueous solution. To

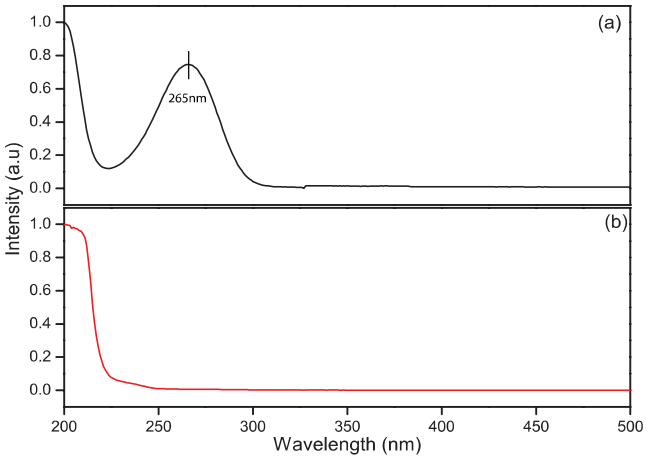

Figure 5.1: UV-Vis spectrum of (a) VA and (b) VL at room temperature in range from 200nm to 800nm on the freshly prepared samples.

compare the optical properties of VA and VL with that of AA and AL, we performed the same experiment on these two samples viz. VA and VL as well. Figure 5.1 (a) shows the normalized UV-Vis spectrum of VA and Figure 5.1(b) for VL at room temperature in the range from 200nm to 800nm. The spectrum of VA shows the increase in absorption below 250nm. The

prominent absorption peak at 265nm corresponding to reducing agent i.e. ascorbate sodium overshadow the absorption due to Si-NPs. In VL, there is a gradual increase in absorption with decreasing wavelength from 250nm. In both VA and VL, the band edge is towards shorter wavelength indicating that we have synthesized smaller particles.

5.1.2 Photoluminescence

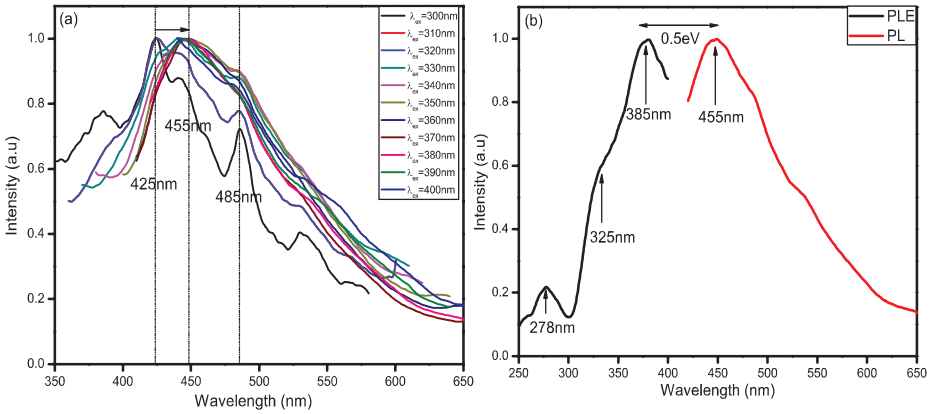

Figure 5.2: (a) PL of VA at room temperature at different excitation wavelength from 300nm to 400nm on the freshly prepared samples, (b) normalized PL and PLE spectra of VA.

As observed from UV-Vis spectra of VA and VL, that both sample absorbed the wavelength below 250nm. In addition, UV irradiation on these Si-NPs also exhibit green fluorescence and can be observed with naked eye. In order to understand and compare the PL properties of VA and VL as well, same excitation range i.e. from 300nm to 400nm were used. The same solution used in the UV-Vis spectroscopy were subsequently used for the PL measurement.

The PL spectra for VA are shown in the Figure 5.2 (a) and for VL in Figure

5.3 (a). In VA, we observed the emission consist of several peaks with two prominent peak centered at 455nm and 485 which can be attributed to presence of various sized nanoparticles in the sample. The PL exhibit blue green emission and the maximum emission was centered around 455nm at an excitation wavelength of 380nm. At lower wavelength excitation i.e. from 300nm to 320nm the shift in the PL spectra were observed from 425nm to 455nm and thereafter no shift in the spectra were observed. The sharp peak at 485nm does not show any shift but however the peak intensity is diminishing with longer wavelength excitation. Along with PL, PLE spectra was recorded by

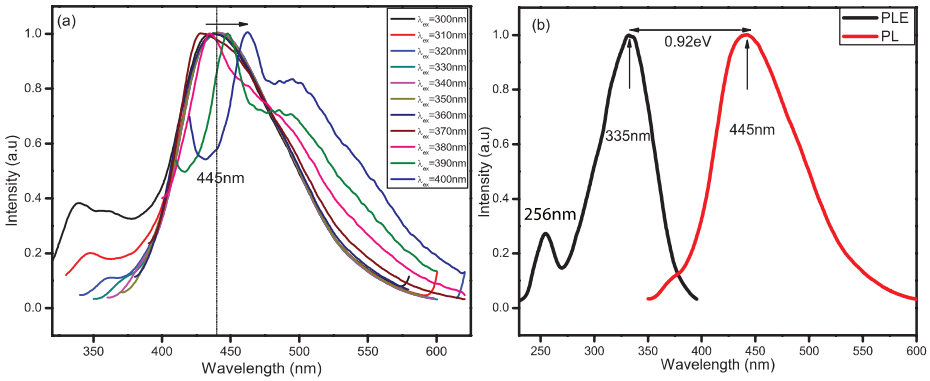

Figure 5.3: (a) PL of VL at room temperature at different excitation wavelength from 300nm to 400nm on the freshly prepared samples, (b) normalized PL and PLE spectra of VL.

monitoring the emission wavelength fixed at 455nm. The normalized PL and PLE spectra are shown in the Figure 5.2 (b). The PLE spectrum in VA has three absorption peaks at 278nm, 325nm and 385nm where we see the maximum absorption. The maximum emission peak at 455nm for VA is due to the PLE peaks at 385nm. The appearance of different emission peak in VA may attributed to three different electronically excited states existed in the

sample and as shown in the PLE spectra [68, 69]. The stokes shift between the emission and absorption band is found to be 0.5eV which indicates that PL in visible region has been originated from the radiative recombination of electron-hole pair from the defect states at the surface of the Si-NPs [63]. Similarly to VA, we have also performed the PL measurement for VL. The PL in VL have been also recorded for excitation wavelength ranging between 300nm to 400nm. The PL spectra of VL shows a gaussian profile in blue green region as well and the maximum emission was centered around 445nm under the excitation wavelength of 330nm. At higher excitation wavelength above 370nm, we observed the shift in the peak position. The normalized PL and PLE spectra are shown in the Figure 5.3 (b). The PLE spectrum in VL has two absorption peaks at 256nm and 335nm. The maximum emission peak at 445nm for VL is the contribution from the PLE peak at 335nm. The stokes shift between the emission and absorption band is found to be 0.92eV. The stokes shift in VL is much larger than VA, therefore we can conclude that the nanoparticles formed in AL are smaller in size as compared to VA. The blue-green emission in both the sample VA and VL is attributed to the same oxide related defect [45].

5.2 Fourier transform infrared spectroscopy

To examine a main chemical bond in these samples, the FTIR spectrum were obtained and measured as well. Figure 5.4 shows the FTIR spectrum of VA and VL in the scanning range from 700cm$^-$1 to 4000cm$^-$1. The sharp absorbance peak at 1018cm^{-1} is ascribed to Si-O-Si bonding in the samples

[65]. The broad absorbance peak at around $1410cm^{-1}$ is due to N-H bending vibration [8]. The absorbance in the range from $2870cm^{-1}$ to $2960cm^{-1}$ is attributed to O-H bond [8]. The broad peak at $920cm^{-1}$ is ascribed to Si-OH bonding [65, 64, 70]. The less prominent peak at $1111cm^{-1}$ is ascribed to SiO_2 [64, 70].

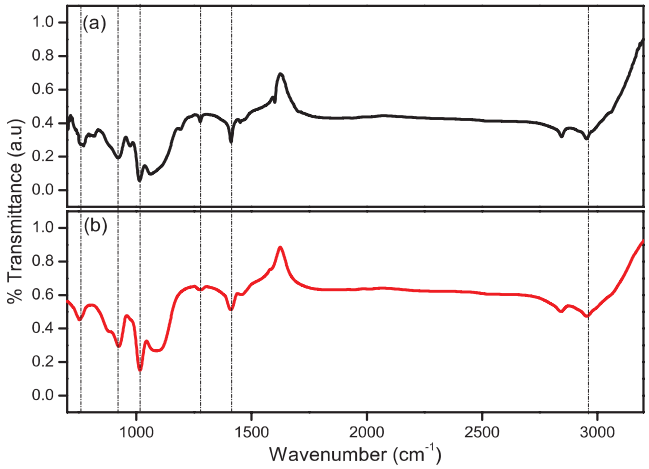

Figure 5.4: FTIR spectrum of VA and VL in the scanning range from 700cm−1 to 4000cm−1 on the freshly prepared samples.

5.3 Transmission electron microscopy

Figure 5.5 shows the TEM images of two samples of Si-NPs viz. VA and VL. It can be seen that the shape of the particles are spherical in VA and nearly spherical in VL. The average diameter of particles are found to be 243nm (± 13nm) for VA and 47nm (± 18nm) for VL. The TEM images were obtained for months old samples and therefore the large sized nanoparticles in VA is due to the agglomeration of synthesized nanoparticles which happens over a

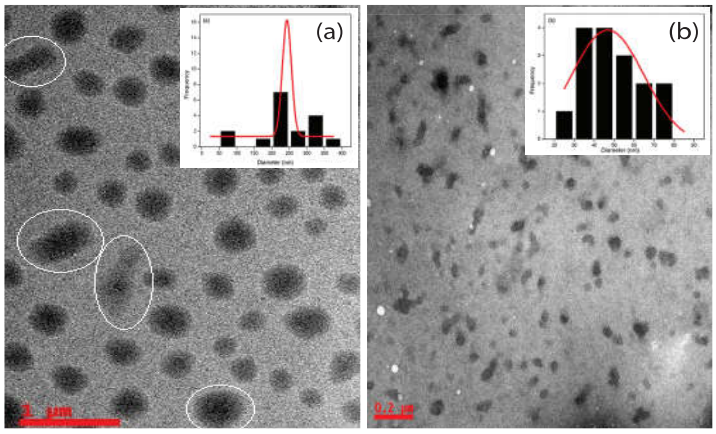

Figure 5.5: Particle sizes analysis histogram of (a) VA showing agglomeration indicated by circle and (b) VL calculated from TEM images

time period. In order to explore its optical behavior we performed the time dependent studies which is detailed in next section.

5.4 Ageing effect on the optical properties of silicon nanoparticles

To check their aqueous stability over a time period we have try to study their optical property of synthesized Si-NPs as function of reduction time.

5.4.1 UV-Vis spectroscopy

Figure 5.6 shows the UV-Vis spectra of (a) VA and (b) VL on 1st, 7th and 14th day of the synthesis in the scanning range from 200nm to 800nm. In VA, the absorption peak at 265nm corresponding to ascorbate sodium decreases but overall the absorption band below 250nm onwards shows small increase in absorption. This may be attributed to the slow reduction process which is

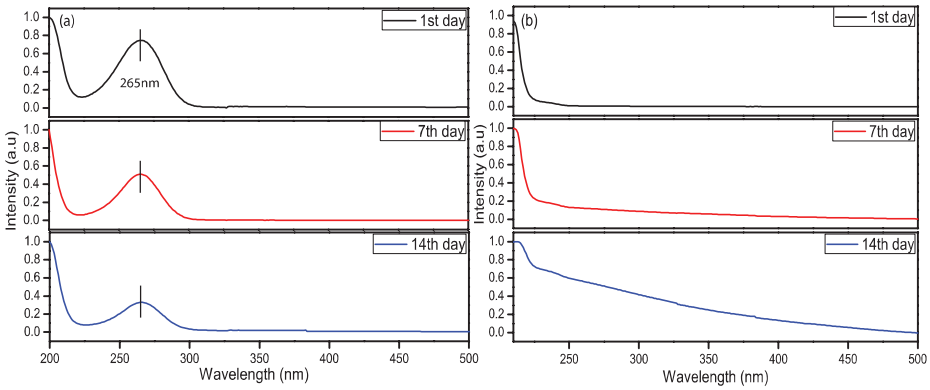

Figure 5.6: UV-Vis spectra of (a) VA and (b) VL on 1st, 7th and 14th day in the scanning range from 200nm to 800nm.

undergoing. In VL, we see the maximum absorption below 250nm on 1st and 7th day of synthesis. On the 14th day enhancement in absorption can be seen from 250nm to 400nm. This may be due to synthesis of more nanoparticles over a time.

5.4.2 Photoluminescence

A time dependent PL studies were performed for these sample VA and VL to investigate their photostability in aqueous medium. For VA and VL, the PL spectra were recorded from 390nm to 600nm using an excitation wavelength of 370nm. The PL spectra for the 1st, 7th and 14th day of synthesized VA are shown in Figures 5.7 (a) and for VL in Figure 5.8 (a).

The emission peak on the 7th and 14th day are red shifted to 485nm by 30nm as compared to 1st day of synthesis. This can be attributed to agglomeration which is happening over a time period in the solution. The same can be seen in the images of TEM for VA (see section 1.3). On fitting the PL spectra, we get two deconvulated gaussian peaks P1 (centered at 455nm) and P2

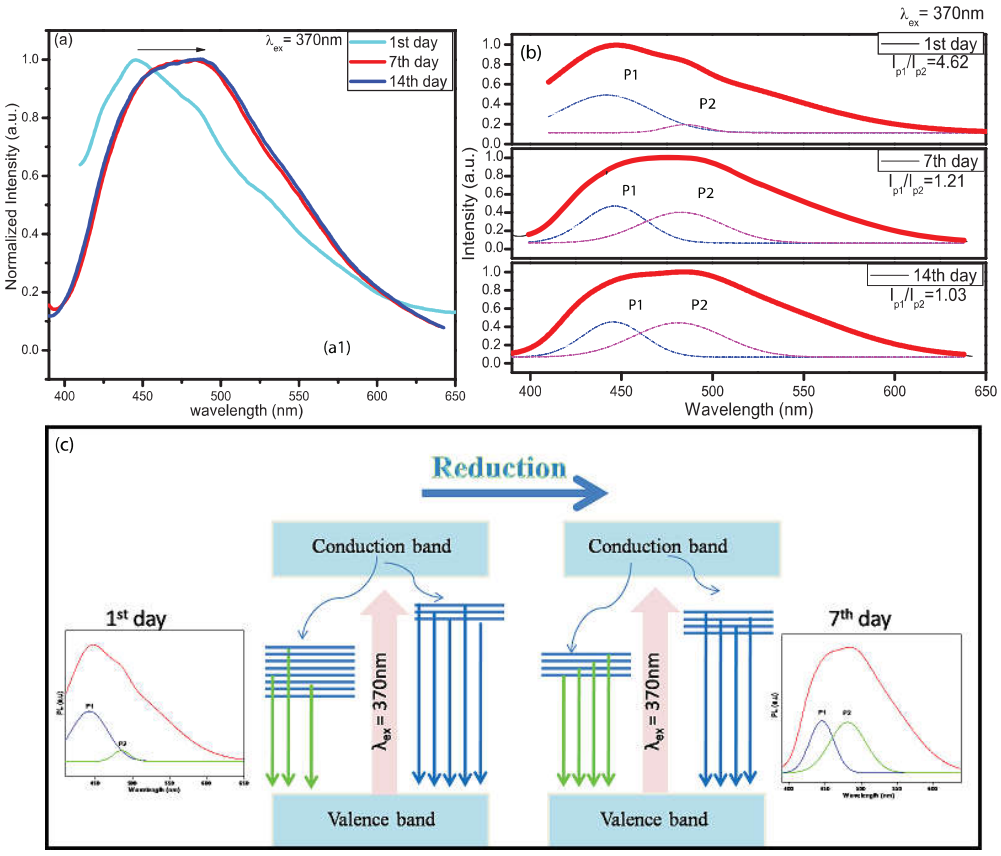

Figure 5.7: PL spectra of (a) VA on 1st, 7th and 14th day in the scanning range from 200nm to 800nm at an excitation wavelength of 370nm, (b) PL spectra of VA with two deconvoluted gaussian band of I_{p1} and I_{p2} as a function of reduction time and pink and blue line are the envelope of deconvulated peaks (c) The proposed PL mechanisms of the predominant I_{P1} emission and I_{P2} emission in AL with green and blue line are the envelope of deconvulated peaks.

(centered at 485nm). With ageing, the increase in intensity of peak P2 were observed whereas the intensity of P1 peak remains almost constant. The PL spectra for the 1st, 7th and 14th day with two deconvulated peaks are shown in Figure 5.7 (b). On the first day of synthesis, the relative intensity ratio, I_{p1} /I_{p2} comes out to be 4.62. The ratio gradually drops and on 14th day the recorded ratio is found to be 1.03. The enhancement in the intensity of P2 which is at longer wavelength reveals the agglomeration process in the solution. PL mechanism in VA using an electronic bandgap is shown in Figure 5.7 (c). On the 1st day of synthesis, the particles emitting at longer wavelength (485nm) having larger bandgap with respect to shorter wavelength (455nm) are minimum in number. With ageing, the particles emitting from defect centres at longer wavelength are increasing. This results indicates the formation of larger particles or possibly the agglomeration were happening over a time period which clearly explain the observed redshift in the spectrum.

The PL spectra in VL were recorded for two different excitation wavelength i.e. 370nm and 300nm. The PL spectra for an excitation wavelength 370nm has been shown in the inset of Figure 5.8 (b). At the excitation wavelength of 370nm, part of emission peak could not be explored for 7th and 14th day. Therefore in order to study the time dependent optical property we have monitor the emission spectra at an excitation wavelength of 300nm. In VL, the peak centered at 445nm on the 1st day of synthesis has been blueshifted to 350nm on the 7th day of synthesis. The blueshift of 95nm can be attributed to synthesis of smaller sized nanoparticles with ageing. On 14th day, no significant change is observed revealing the stability of synthesized nanoparticles. The curve fitting of PL spectra shows the presence of two

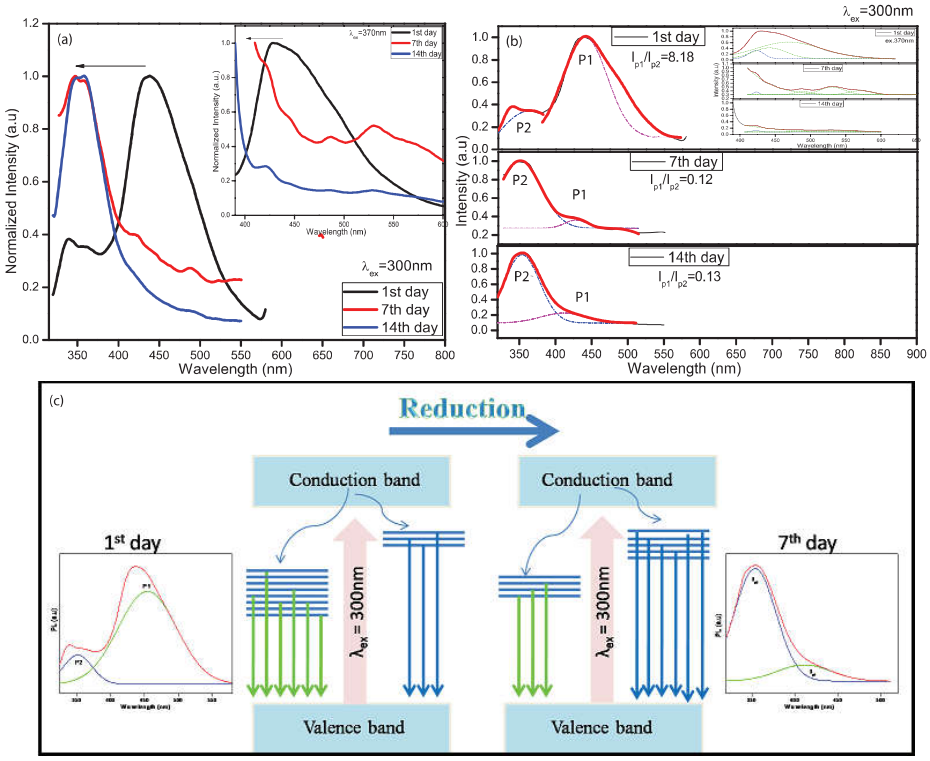

Figure 5.8: PL spectra of (a) AL on 1st, 7th and 14th day in the scanning range from 200nm to 800nm at an excitation wavelength of 370nm, (b) PL spectra of AL with two deconvoluted gaussian band of I_{p1} and I_{p2} as a function of reduction time and pink and blue line are the envelope of deconvulated peaks (c) The proposed PL mechanisms of the predominant I_{P1} emission and I_{P2} emission in AL with green and blue line are the envelope of deconvulated peaks.

deconvulated peaks having centered at 445nm (P1) and 350nm (P2). On the 1st day of synthesis, the PL is wholly contributed from the emission centered at P1. The observed relative intensity ratio I_{p1} /I_{p2} found out to be 8.18. With ageing, the relative intensity rapidly drops to 0.13 on the 7th and remain same for 14th day. The rapid fall in the relative intensity ratio and the ratio remaining same on the 7th and 14th day indicates the fast and complete reduction process that has taken place. The PL mechanism for this sample have also been explained on the basis of electronic bandgap as shown in Figure 5.8 (c). As seen from the figure, the particles emitting at longer wavelength (445nm) having smaller bandgap on the 1st day are huge in number with respect to particles emitting at shorter wavelength (350nm) having larger bandgap. On 7th day, the particles emitting at shorter wavelength has increased rapidly and proportionally with respect to the decreased in the particles emitting at longer wavelength. This results clearly indicates the formation of smaller sized nanoparticles from larger sized nanoparticles with ageing time. This results explain the shifting of PL peak in VL with ageing. The two samples VA and VL shows opposite behavior with ageing. With ageing in VA, we can see redshift because of synthesis of nanoparticles which are not stable in the solution and shows agglomeration verified by PL and TEM images. In contrary in VL, we see blueshift because of reduction of large Si-NPs (emitting at 445nm) to small sized nanoparticles (emitting at 350nm). The sample AA and VA prepared using reducing agents ascorbate sodium lead to the redshifted and the sample AL and VL prepared using *Citrus lemon* extract were seen to be blueshifted. This analysis strongly support that *Citrus lemon* is a better reducing agent than ascorbate sodium.

5.5 Fourier transform infrared spectroscopy

Figure 5.9 shows the FTIR spectrum of (a) VS and (b) VL on 1st, 7th and 14th day of synthesis. The absorbance peak at $1018cm^{-1}$ which has been ascribed to Si-O-Si bonding has become enhanced with ageing and become a sharp peak by the 7th day in both samples. The broad peak at $920cm^{-1}$ which is ascribed to Si-OH bonding disappeared completely by the 14th day. The less prominent peak at $1111cm^{-1}$ ascribed to SiO_2 remained over a time period in both the samples. The absorbance at around $1410cm^{-1}$ which is due to N-H bending vibration remain the same over a time period.

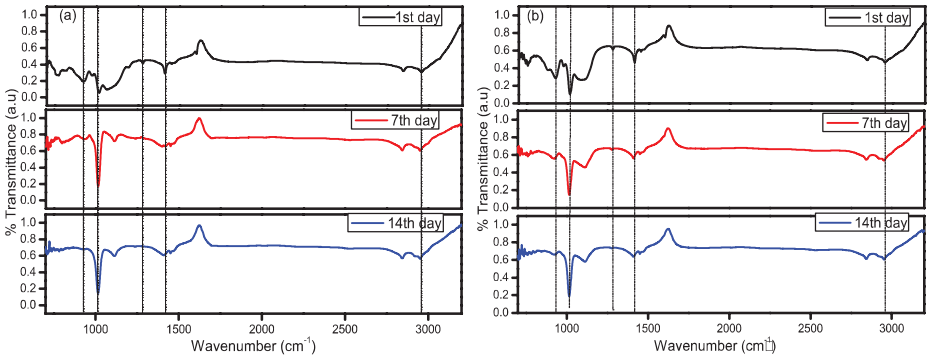

Figure 5.9: FTIR spectra of (a) VA and (b) VL on the 1st, 7th and 14th day in the scanning range from 700cm−1 to 4000cm−1.

Part V

Results and Discussion

Chapter 6

Silicon nanoparticles as a fluorescence probe

In this chapter we have try to explore the efficiency of the synthesized Si-NPs as a fluorescence probe in bioimaging techniques. The fluorescence imaging were performed on human WBCs using Si-NPs viz. VA and VL. The materials and methods adopted for this experiment have been detailed in the chapter materials and method. The cells which were seeded in dishes containing DMEM medium stained with two different concentration Si-NPs viz. $6.16\,\mu g\,ml^{-1}$ and $1.54\,\mu g\,ml^{-1}$ were incubated in a fully humidified incubator at 37°C with 5% CO_2 for 1.5 h. After the incubation the cell were ready for imaging measurements. The cells stained with different concentration of Si-NPs were used for cell imaging. The concentration of silicon precursor were calculated assuming that there is a complete reduction of silicon precursor. The fluorescence imaging were performed with two different light illumination viz. green and UV light. Figure 6.1 shows the controlled cell

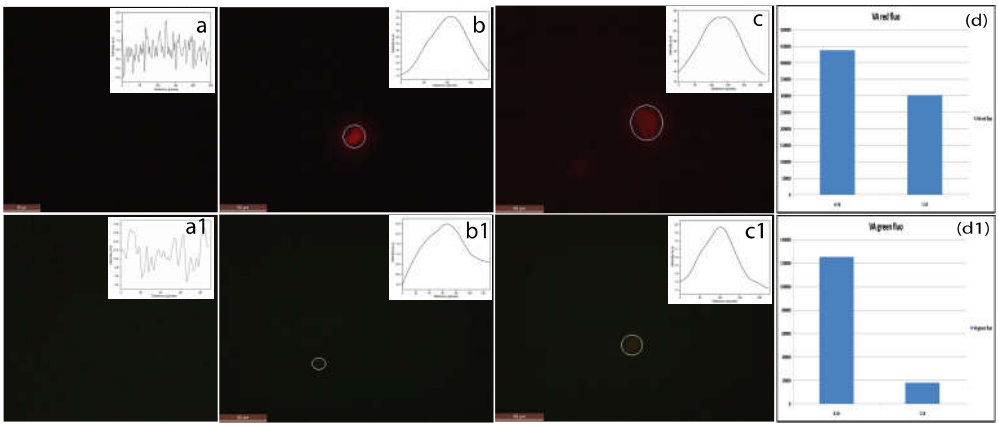

Figure 6.1: Controlled cell images at an excitation wavelength (a) green and (a1) UV light. Red fluorescence emission (b,c) using green excitation wavelength and green fluorescence emission (b1,c1) using UV excitation of human WBCs cell stained with VA at two different concentration. CTCF graph for VA for (d) red fluorescence and (d1) green fluorescence at two different concentration

images of human WBCs without staining under (a) green and (a1) UV illumination. Here under both the illumination, no fluorescence can be seen. By staining human WBCs cell with Si-NPs (VA) and illuminating with green light, we see the fluorescence in red region. The images obtained are shown in the Figure 6.1 (b) and (c) for two different concentration of Si-NPs. In the inset of each figure we have shown the fluorescence intensity profile taken across the cross section of the fluoresced cell as indicated by the circle in the images. By illuminating the same sample with UV light, we see the green fluorescence. The images are shown in the Figure 6.1 (b1,c1) obtained for two different concentration. Here we try to measure the level of cell fluorescence in a given region. For measurement we have used Imagej software and the following steps were as followed [71].

1. Selected the fluoresced cell stained with nanoparticles.

2. From the selected area we have determine integrated density and mean gray value.

3. Then we select the region next to fluoresced cell with no fluorescence for background.

4. Then we used the following formula to calculate the corrected total cell fluorescence (CTCF).

CTFC=Integrated density - (area of selected cell- mean fluorescence of background readings).

The Figure 6.1 (d) and (d1) shows the CTCF of cell with two different concentration and at two different light illumination. As seen from the Figure, the fluorescence intensity increases with increase in concentration in both the sample.

Similarly for VL, the fluorescence imaging were performed with two different

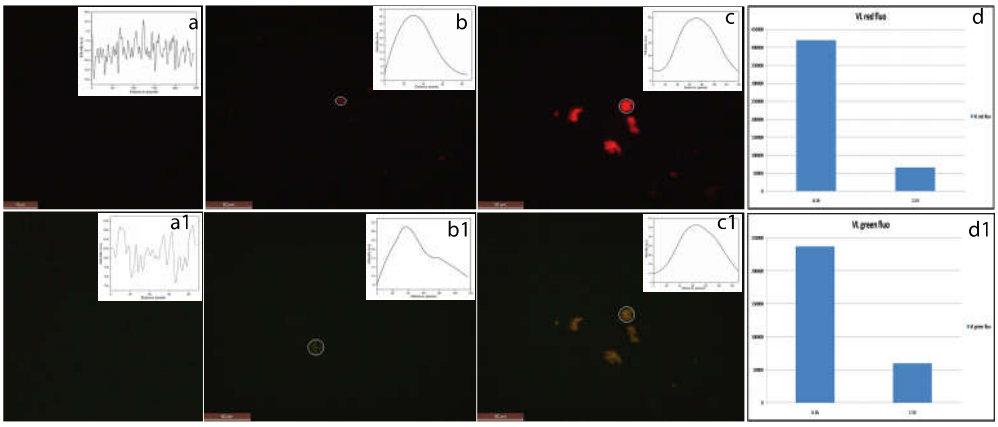

Figure 6.2: Controlled cell images at an excitation wavelength (a) green and (a1) UV light. Red fluorescence emission (b,c) using green excitation wavelength and green fluorescence emission (b1,c1) using UV excitation of WBC stained with VL at two different concentration. CTCF graph for VA for (d) red fluorescence and (d1) green fluorescence two different concentration

Table 6.1: Red and green CTCF at two different concentration for VA and VL

Sample	Red CTCF		Green CTCF	
	$6.16\,\mu g\,ml^{-1}$	$1.54\,\mu g\,ml^{-1}$	$6.16\,\mu g\,ml^{-1}$	$1.54\,\mu g\,ml^{-1}$
VA	438151	301383	125302	17905
VL	419190	65285	236772	59611

light illumination viz. green and UV light. Figure 6.2 shows the controlled cell images of human WBCs without staining under (a) green and (a1) UV illumination. Similar to VA, in this case also under green illumination we see the red fluorescence. The images obtained are shown in the Figure 6.2 (b) and (c) for two different concentration of Si-NPs. In the inset of each figure we have shown the fluorescence intensity profile taken across the cross section of the fluoresced cell as indicated by the circle in the images. By illuminating the same sample with UV light, we see the green fluorescence. The images are shown in the Figure 6.2 (b1,c1) obtained for two different concentration. In this case also we see the same trend as VA. With increase in concentration, fluorescence is increasing in both the sample i.e. VA and VL as shown by red and green CTCF data which are given in the Table 6.2.

The red CTCF value obtained for VA and VL at higher concentration is found to be 438151 and 419190 which shows that the level of cell fluorescence is almost same in VA and VL. But the level of red CTCF decrease in VL at lower concentration by a factor of 5 than VA. The green fluorescence in both the sample are less intensified compared with the red fluorescence. But the level of green CTCF are not same in both the samples. The green CTCF in VL are greater than by a factor of 2 than VA. A more number of cell fluoresces under VL staining which is probably due to a number of cells

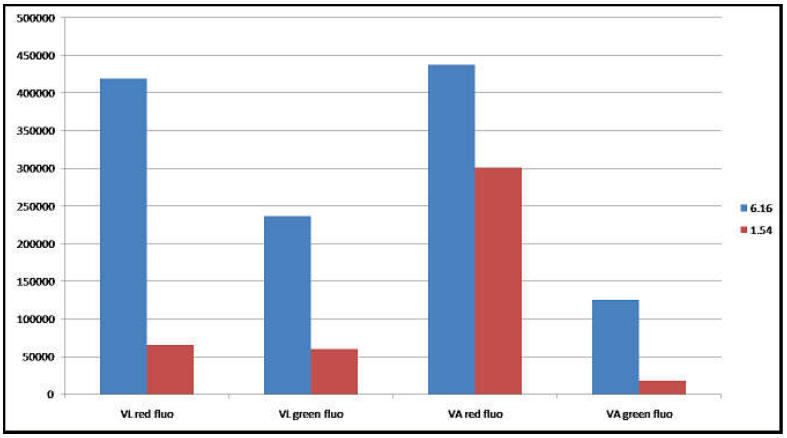

Figure 6.3: CTCF graph representing the level of fluorescence in VA and VL for two different concentration and at two different light illumination.

undergoing possible nucleated staining with VL than with VA. This suggest that the efficiency of smaller Si-NPs as s fluorescence probe is better as compared to larger one. This results indicate that VL is a better fluorescence probe than VA for their use in biological imaging.

Chapter 7

Silicon nanoparticles as an antimicrobial agent

7.1 Effect of silicon nanoparticles against Bacteria and Fungi

The antimicrobial activity of silicon nanoparticle samples viz. AA, AL, VA and VL were assessed by disc diffusion method against following test organisms: *Escherichia coli* MTCC 739, *Escherichia coli* MTCC 10312, *Bacillus subtilis MTCC* 441, *Bacillus subtilis* MTCC 2757, *Candida albicans* MTCC 227 and *Trichophyton rubrum* ANTR01. Inhibition zones of the test samples are shown in Table 7.1.

Test samples, AA and AL were found to show antimicrobial activity against both strains of gram negative bacteria viz.*Escherichia coli* MTCC 739 and *Escherichia coli* MTCC 10312; both strains of gram positive bacteria viz.

Table 7.1: Antimicrobial activity of silicon nanoparticles against various test organisms at different concentration and their corresponding MIC values

Samples	Conc.of samples	Gram positive bacteria		Gram negative bacteria		Fungi	
		Bacillus subtilis MTCC 441 (mm)	*Bacillus subtilis* MTCC 2757 (mm)	*E.coli* MTCC 739 (mm)	*E.coli* MTCC 10312 (mm)	*Candida albicans* MTCC 227 (mm)	*Trichophyton rubrum* ANTR01 (mm)
AA	7.61 µg ml^{-1}	21.3	20.0	16.6	12.5	13.5	Nil
	3.81 µg ml^{-1}	15	15.5	12.6	10.0	9.0	Nil
	1.90 µg ml^{-1}	12.5	10.5	Nil	Nil	Nil	Nil
AL	7.61 µg ml^{-1}	13.5	16.0	10.0	12.5	9.0	Nil
	3.81 µg ml^{-1}	11.5	11.5	Nil	Nil	Nil	Nil
	1.90 µg ml^{-1}	Nil	Nil	Nil	Nil	Nil	Nil
VA	6.16 µg ml^{-1}	Nil	Nil	Nil	Nil	Nil	Nil
	3.08 µg ml^{-1}	Nil	Nil	Nil	Nil	Nil	Nil
	1.54 µg ml^{-1}	Nil	Nil	Nil	Nil	Nil	Nil
VL	6.16 µg ml^{-1}	11.5	Nil	Nil	Nil	Nil	Nil
	3.08 µg ml^{-1}	9.5	Nil	Nil	Nil	Nil	Nil
	1.54 µg ml^{-1}	Nil	Nil	Nil	Nil	Nil	Nil

Bacillus subtilis MTCC 441 and *Bacillus subtilis* MTCC 2757; one strain of Candida viz. *Candida albicans* MTCC 227. The Figure 7.1 and 7.2 shows the antimicrobial activity exhibited by AA and AL in both strain of gram positve and gram negative bacteria. The Figure 7.3 shows the antimicrobial activity of AA and AL in *Candida albicans*. None of the test samples showed inhibition against *Trichophyoto rubrum* ANTR01. VL was found to show inhibition against only one strain of bacteria viz. *Bacillus subtilis* MTCC 441. The Figure 7.4 shows the antimicrobial activity of VL in *Bacillus subtilis* MTCC 442. VL and VA were found to be ineffective against rest of the test organisms. The MIC values of AA is found to be 1.90g/mL in both strain of gram positive bacteria and 3.81g/mL in both strain of gram negative bac-

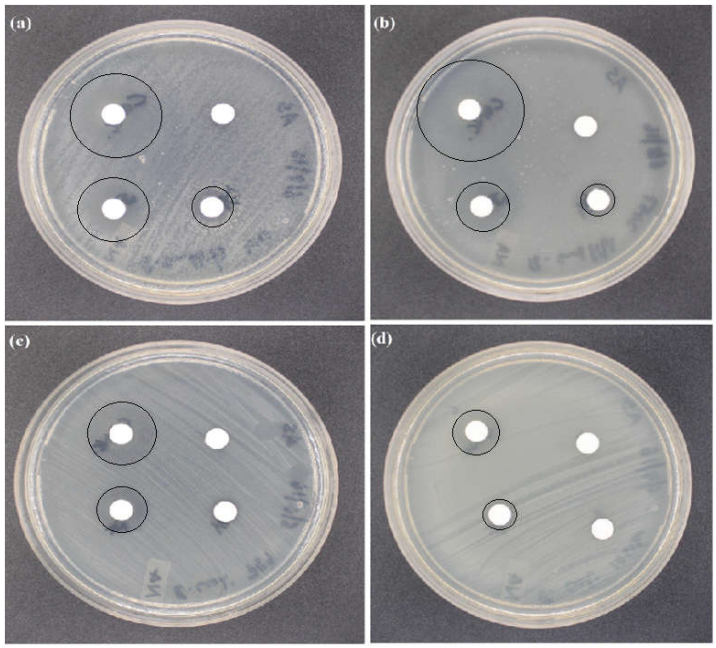

Figure 7.1: Antimicrobial activity shown by AA in (a) *Bacillus subtilis* MTCC 442, (b) *Bacillus subtilis* MTCC 2757, (c) *Escherichia coli* MTCC 739 and (d)*Escherichia coli* MTCC 10312.

teria as well as in *Candida albicans* MTCC 227. Similarly, the MIC values of AL is found out to be 3.81g/mL in both strain of gram positive bacteria and 7.61g/mL in both strain of gram negative bacteria as well as in Candida albicans MTCC 227. The MIC values of VL is found out to be 3.08g/mL in *Bacillus subtilis* MTCC 44. The antimicrobial activity of four samples for the test microorganism has been given in the following figures.

Among the four samples, AA and AL were found to show higher antimicrobial activity against test microorganisms. The zone of inhibition in case of AA as shown in the table 2 as compared to other samples is twice as large as in case of *Bacillus subtilis* MTCC 441 at a concentration of 7.61g/mL. The most sensitive microorganism was *Bacillus subtilis* MTCC 441, which was

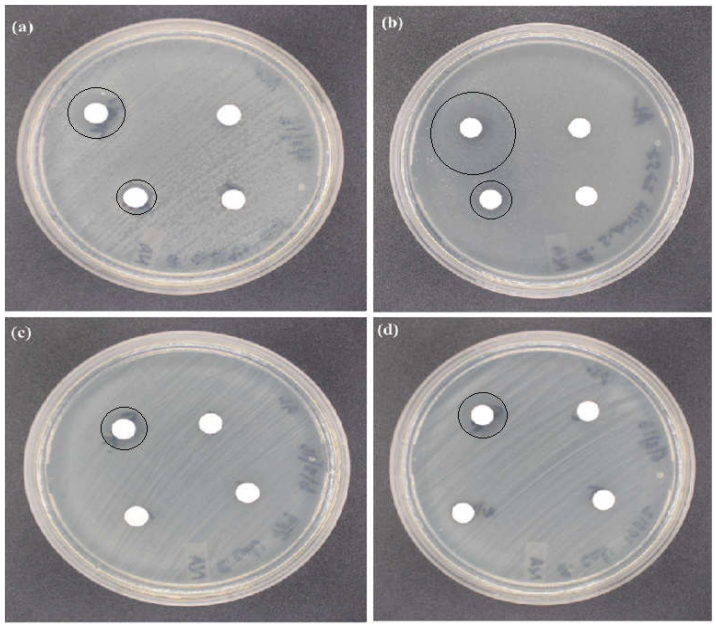

Figure 7.2: Antimicrobial activity showed by AL in *Bacillus subtilis* MTCC 442, (b) *Bacillus subtilis* MTCC 2757, (c) *Escherichia coli* MTCC 739 and (d)*Escherichia coli* MTCC 10312.

susceptible to all the samples at various dilution except for VA. The samples AA and AL showed higher efficacy against test pathogens is due to the fact that the both samples have been prepared from 3aminopropyltrimethoxysilane which has greater efficacy than VS and VL which has been prepared from Venytrimethoxysilane. In addition, AA and AL has smaller particle size than VA and VL as confirmed from TEM analysis that allows them to disperse or penetrate in media more effectively. The faster rate of diffusion of smaller particles allows for a more rapid association with bacteria.

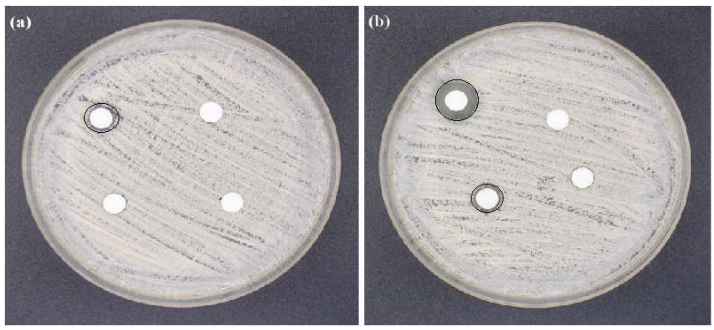

Figure 7.3: Antimicrobial activity shown by (a) AL and (b) AS in *Candida Albicans* MTCC 227

Figure 7.4: Antimicrobial activity shown by VL in *Bacillus Subtilis* MTCC 442

Part VI

Conclusion and Future prospects

Chapter 8

Conclusion and Future prospects

8.1 Conclusion

The nobel features of Si-NPs such as large surface area, tunable PL and excellent biocompatibility offer great advantage. The Si-NPs using functionalized groups imparts desirable properties for the use in biomedical applications especially as a fluorescence probe. Therefore numerous research has focussed in studying its optical, physical and biological properties. Here we try to study the optical and biological properties of four different samples of Si-NPs. Herein we synthesized Si-NPs that are water dispersible, hydrophilic and transparent aqueous solution and no turbidity were seen. The PL of all four samples emit in blue-green region inspite having larger particles size as confirmed by the TEM analysis. The FTIR spectra of all four samples shows the formation of siloxane (Si-o-Si) and Si-O bond in the samples. These

analysis confirms the origin of PL in our sample are not from the quantum confinement effect but rather from the localized state induced by the surface oxidation. The optical properties of sample AA and VA follows the similar behaviour with ageing. The sample have been prepared from different precursor but the reducing agents used is same which implies that the appearance of similar behaviour in both the samples are the consequences of type of reducing agent. The spectrum shows broad distribution with ageing in both the samples which does not make ascorbate sodium an effective reducing agents. Similarly, the optical properties of sample AL and VL shows the similar behaviour. The PL and absorption peak moves towards shorter wavelength in both the samples with ageing which implies that *Citrus Lemon* extract is a good reducing agents. Although, the PL shift in freshly prepared AL with different applied excitation wavelength is also noticeable but with ageing the sample show stability in PL as observed on the 7th day. The PL spectrum are narrow in AL and VL as compared to AA and VA. The large stokes shift in both the sample AL and VL further suggest the formation of smaller sized nanoparticles in this case as compared to AA and VA. The large stokes shift enables collection of whole emission spectra thereby improving its sensitivity of detection for biological applications [3]. The bioimaging of two samples of Si-NPs viz. VA and VL were performed on the human WBCs cell. The cell stained with VL and VA shows the same level of red CTCF intensity but the smaller size of VL facilitates the fluorescence of more number of cell. This is because the Si-NPs prepared using *Citrus lemon* are smaller in size as compared to Si-NPs prepared using ascorbate sodium. This results indicates that VL is the better fluorescence probe than VA. In addition we

try to explore other medicinal uses of Si-NPs as antimicrobial agents. The antimicrobial activity of all four samples were performed. The samples AA and AL showed higher antimicrobial activity against test pathogens and VL showed efficacy against one strain of bacteria. From this we find that AA and AL are an effective antimicrobial agents.

8.2 Future prospects

Nanomaterials have become important materials in rapidly growing field of nanotechnology [72]. The size dependent optical properties of Si-NPs finds its application not only in optoelectronics but in biomedical applications. They are basically considered as a new generation fluorescence probe by replacing the conventional dyes used in diagnostics purposes in coming near future. The numerous synthesis route for the preparation of Si-NPs has improved significantly over the past 50 years [73].The synthesis method has undergone major changes which focusses on the fast and high production of nanoparticles useful in the biomedical application. There is an increasing interest in nanomedicine due to their robust and biocompatible nature of Si-NPs. The quantum yield (QY) in Si-NPs were found to be high as compared to CdSe QDs but its surface chemistry and luminescence process is not yet well understood to consider as ideal fluorophore [74]. Si-NPs are recently using for drug and gene delivery due to its low inherent toxicity than their counterparts QDs. Also due to their desired physiochemical property they are considerably studying for their waste water treatment technology [75].

Bibliography

[1] L. T. Canham. "Silicon quantum wire array fabrication by dissolution of wafers". *Appl. Phys. Lett*, 57:1046–1048, 1990.

[2] N. V. Tarasenko M. Mardanian, A. A. Nevar. "Optical properties of silicon nanoparticles synthesized via electrical spark discharge in water". *Appl. Phys. A*, 112:437–442, 2013.

[3] B. R Horrocks N. O. Farrell, A. Houlton. "Silicon nanoparticles: applications in cell biology and medicine". *International Journal of Nanomedicine*, 1(4):451–472, 2006.

[4] D.petrova T. Jamieson, R. Bakshi and R. pocock. "Biological applications of quantum dots". *Biomaterials*, 28:4717–4732, 2007.

[5] y. Gao L. Shao and F. Yan. "Semiconductor quantum dots for biomedical applications". *Sensors*, 11:11736–11751, 2011.

[6] T. Pellegrino W. J. Parak and C. Plank. "Labelling of cell with quantum dots". *Nanotechnology*, 16:9–25, 2005.

[7] W. C. W. Chan A. M. Derfus and S. N. Bhatia. "Probing the cytotoxicity of semiconductor quantum dots". *Nanoletters*, 4:11–18, 2004.

[8] G. H. Liang J. Chang J. L. Kong J. Wang, D. X. Ye and J. Y. Chen. "One-step synthesis of water-dispersible silicon nanoparticles and their use in fluorescence lifetimen imaging of living cells". *J. Mat. Chem. B*, 2:4338–4345, May 2014.

[9] L. A. Blackb J. B. A. Rossb K. Fichterc T. Vuc E. Richmand B. A. Manhata, A. L. Browna and A. M. Gofortha. "One-step melt synthesis of water soluble, photoluminescent,surface-oxidized silicon nanoparticles for cellular jmaging applications". *Chem Mater*, 23(9):2407–2418, May 2011.

[10] A. Pietzsch F. Hennies Y. Bao Y. Chao Q. Wang, H. Ni. "Synthesis of water-dispersible photoluminescent silicon nanoparticles and their use in biological fluorescent imaging". *J Nanopart Res*, 13:405413, 2011.

[11] J. A. Novak M. A. Walling and J. R.E Shepard. "Quantum dots for live cell and in vivo imaging". *Int. J. Mol. Sci*, 10:441–491, 2009.

[12] "http://www-opto.e-technik.uni-ulm.de/lehre/cs/DOS-DIM.jpg".

[13] "nanotech.fzu.cz/26/index.php file=1".

[14] M. M. Golzan M. Farasat. "Preparation and characterization of methyltrimethoxysilane-Ag nanoparticles using chemical reduction at room temperature". *Appl Nanosci*, 4:293–297, 2014.

[15] V. Lysenko G. Bremond J. M. Bluet Y. V. Ryabchikov, S. A. Alekseev. "Photoluminescence of silicon nanoparticles chemically modified by

alkyl groups and dispersed in low-polar liquids". *J Nanopart Res*, 15(1535):1–9, 2013.

[16] V. G. Kravets. "Silicon nanoparticles: their photoluminescence, complex refractive index, and relationship with the band structure". *Optics and Spectroscopy*, 114(2):230235, 2013.

[17] V. Pustovoy A. Surkov E. Kelm, S. Korovin and A. Vladimirov. "Luminescent silicon nanoparticles with magnetic properties-production and investigation". *Appl. Phys. B*, 105:599–606, 2011.

[18] M. Baalousha T. Hofmann P. Christian, F. V. D.Kammer. "Nanoparticles: structure, properties, preparation and behaviour in environmental media". *Ecotoxicology*, 17:326–343, 2008.

[19] Q.S. Li Q. Wu, X. Wang and R.Q. Zhang. "Excited State Relaxation and Stabilization of Hydrogen Terminated Silicon Quantum Dots". *J Clust Sci*, 24:381–397, 2013.

[20] K. Vithiya and S. Sen. "Biosynthesis of nanoparticles". *IJPSR*, 1(11):2781–2785, 2011.

[21] S. Marathe A. Ethiraj N. Hebalkar S. W. Gosavi J. Urban S .K. Kulkarni M. Bangal, S. Asthaputre. "Semiconductor nanoparticles". *Hyperfine Interactions*, 160:81–94, 2005.

[22] K. Kimura. "Blue Luminescence from Silicon Nanoparticles Suspended in Organic Liquids". *J. Clust Sci*, 10(2):359–380, 1999.

[23] K. Hanaka K. suzuki A. Shiohara, A. Hoshino and K. yamamoto. "On the cyto-toxicity caused by quantum dots". *Microbiol. Immunol*, 48:669–675, 2004.

[24] D. Petrova R. Pocock M. Imani T. Jamieson, R. Bakhshi and A. M. Seifalian. "Biological applications of quantum dots". *Biomaterials*, 28:4717–4732, 2007.

[25] D. Munao A. Evirgen E. M. Kelder A. S. Ott V. A. Vons, L. C. P. M. Smet. "Silicon nanoparticles produced by spark discharge". *J Nanopart Res*, 13:4867–4879, 2011.

[26] E. R. Andreevaa L. B. Buravkovaa A. N. Shubenkova, S. B. Korovinb and V. I. Pustovoyb. "In vitro Evaluation of Crystalline Silicon Nanoparticles Cytotoxicity". *Biophysics*, 59(1):105–109, 2014.

[27] L. T. Canham A. G. Cullis and P. D. J. Calcott. "The structural and luminescence properties of porous silicon". *J. Appl. Phys*, 82(3):909–965, 1997.

[28] E. Rani A. Ingale A. K. Srivastava L. M. Kukreja A. Chaturvedi, M. P. Joshi. "On red-shift of UV photoluminescence with decreasing size of silicon nanoparticles embedded in SiO2 matrix grown by pulsed laser deposition". *Journal of Luminescence*, 154:178–184, 2014.

[29] P. T. Kalaichelvan S. Rana. "Antimicrobial activities of metal nanoparticles". *Advanced Biotech*, 11(2):21–23, 2011.

[30] A. W. Xu G. Q. Chang Z. J. Hu W. L. He Z. H. Xing J. B. Xu M. Wang T. Y. Cheang, B. Tang and S .M . Wang. "Promising plasmid DNA vector based on APTES-modified silica nanoparticles". *International Journel of Nanomedicine*, 7:1061–1067, 2012.

[31] R. M. Clegg D. A. Eckhoff, J. D. B. Sutin and E. Gratton. "Optical characterization of ultrasmall Si nanoparticles prepared through electrochemical dispersion of bulk Si". *J. Phys. Chem*, 109:19786–19797, 2005.

[32] J. Zou and S. M. Kauzlarich. "Functionalization of silicon nanoparticles via silanization: alkyl, halide and ester". *J Clust Sci*, 19:341–355, 2008.

[33] K. Yoshida I. Umezu A. Sugimura T. Makino, M. Inada. "Structural and optical properties of silicon nanoparticles prepared by pulsed laser ablation in hydrogen background gas". *Appl. Phys. A*, 79:1391–1393, 2004.

[34] T. Takahashi K. Murakami T. Makimura, T. Mizuta. "In situ size measurement of Si nanoparticles and formation dynamics after laser ablation". *Appl. Phys. A*, 79:819–821, 2004.

[35] J. J. Chiu H. S. Chaen and T. P. Perng. "On the photoluminescence of Si nanoparticles". *Mter. Phys. Mech*, 4:62–66, 2001.

[36] R. M. Williams S. W. Clark M. P. Bruchez F. W. Wise D. R. Larson, W. R. Zipfel and W. W. Webb. "Water soluble quantum dots for multiphoton fluorescence imaging in vivo". *Science*, 2003.

[37] P. Sharma S. C. Brown B. M. Moudgil M. A. Hahn, A. K. Singh. "Nanoparticles as contrast agents for in-vivo bioimaging:current status and future perspectives". *Anal Bioanal Chem*, 399:3–27, 2011.

[38] "Hanbook of thin films materials". *Nanomaterials and magnetic thin films*, 5, 2002.

[39] G. Walter S. Santra P. Sharma, S. Brown and B. Moudgil. "Nanoparticles for bioimaging". *Advances in colloid and interface sciences*, 123-126:471–485, 2006.

[40] F. Pevere Z. Yang I. Sychugov, A. Fucikova and J.G..C. Veinot. "Ultranarrow luminescence linewidth of silicon nanocrystals and influence of matrix". *ACS photonics*, 1:998–1005, 2014.

[41] K. Yamamoto R. D. Tilley J. H. Warner, A. Hoshino. "Water soluble photoluminescent silicon quantum dots". *Angew. Chem. Int. Ed*, 44:2–6, 2005.

[42] W. Perrie S. Romani R. J. Potter S. P. Edwardson P. French M. Sharp G. Dearden K. G. Watkins N. G. Semaltianos, S. Logothetidis. "Silicon nanoparticles generated by femtosecond laser ablation in a liquid environment". *J Nanopart Res*, 12:573–580, 2010.

[43] an P. M. Fauchet M. V. Wolkin, J. Jorne. "Electronic states and luminescence in porous silicon quantum dots: the role of oxygen". *Physical review letter*, 82(1):197–200, January 1999.

[44] F. Huisken O. Guillois G. Ledoux, J. Gong and C. Reynaud. "Photoluminescence of size-separated silicon nanocrystals: Confirmation of quantum confinement". *Applied Physics Letters*, 80(25), 2002.

[45] T. Kishi M. Hirai H. Suematsu W. Jiang X. P. Zhu, T. Yukawa and K. Yatsui. "Synthesis of light-emitting silicon nanoparticles by intense pulsed ion-beam evaporation". *Journal of Nanoparticle Research*, 7:669–673, 2005.

[46] E. Gratton E. V. Rogozhina, D. E. Eckhoff and P. Braun. "Carboxyl functionalization of ultrasmall luminescent silicon nanoparticles through thermal hydrosilylation". *J. Mater. Chem*, 16:1421–1430, 2006.

[47] W. J. Cho T. W. Kim D. H. Oh, S. Lee. "Effects of hydrogenation and aging on the optical properties in porous Si layers". *J Mater Sci*, 42:6862–6865, 2007.

[48] S. Luttjohann C. Meier, A. Gondorf and A. Lorke. "Silicon nanoparticles: Absorption, emission, and the nature of the electronic bandgap". *J. Appl. Phys*, 101(103112), 2007.

[49] A. Henglein A. Fojtik. "Luminescent colloidal silicon nanoparticles". *Chem. Phy. Lett*, 221:363–367, 1994.

[50] F. M. Petrat U. Simon J. Nelles, D. Sendor. "Electrical properties of surface functionalized silicon nanoparticles". *J Nanopart Res*, 12:1367–1375, 2010.

[51] R. Karimzadeh M. Amini N. Mansour, A. Momeni. "Blue-green luminescent silicon nanocrystals fabricated by nanosecond pulsed laser ablation in dimethyl sulfoxide". *Optical materials express*, 2(6):740–748, June 2012.

[52] K. Murakami T. Makimura, T. Mizuta. "Formation process of Si nanoparticles in rare gas observed by a decomposition method". *Appl. Phys. A*, 69:213–215, 1999.

[53] A. B. Evlyukhin T. Birr B. N. Chichkov U. Zywietz, C. Reinhardt. "Generation and patterning of Si nanoparticles by femtosecond laser pulses". *Appl. Phys. A*, 114:45–50, 2014.

[54] A. A. Ishchenkoc R. B. Vasil M. A. Goldschtrakhc K. V. Zaitsevac V. V. Koltasheve V. G. Plotnichenkoe S. G. Dorofeeva, N. N. Kononovb and O. V. Tikhonevich. "Optical and structural properties of thin films precipitated from the sol of silicon nanoparticles". *Semiconductors*, 43(11):1420–1427, 2009.

[55] J. M. Mauro J. K. Jaiswal, H. Mattoussi and S.Simon. "Long term multiple color imaging of live cell using quantum dot bioconjugates". *Nature biotechnology*, 21:47–51, 2003.

[56] G. S. Alvareza A. M. Meberta L. E. Diaza T. Coradinb D. E. Camporotondia, M. L. Fogliaa and M. F. Desimonea. "Antimicrobial properties of silica modified nanoparticles". *Appl. Phys. A*, 114:45–50, 2013.

[57] X. Wang J. Hu H. Lu, H. Mo. "The Broad-spectrum antimicrobial activity and biocompatibility of the mesoporous silica nanoparticles encapsu-

lated with silver nanocrystals". *European Cells and Materials*, 28(5):30, 2014.

[58] A. Dong Q. Dong and Morigen. "Evaluation of novel antibacterial N-Halamine nanoparticles prodrugs towards susceptibility of escherichia coli Induced by DksA protein". *Molecules*, 20:7292–7308, 2015.

[59] H. S. Paul M. H. Schoenfisch E. M. Hetrick, J. H. Shin. "Anti-biofilm efficacy of nitric oxide-releasing silica nanoparticles". *Biomaterials*, 30:2782–2789, 2009.

[60] G. Wilde M. S. Wafaa A. Khayat. "Characteristics study of silicon nanoparticles produced by physical vapour deposition". *American Journal of Materials Science*, 2(6):210–214, 2012.

[61] F. Fabbri V. Bello E. Borsella R. D. Amato, M. Falconieri. "Preparation of luminescent Si nanoparticles by tailoring the size, crystallinity and surface composition". *J Nanopart Res*, 12:1845–1858, 2010.

[62] C. Rajesh S. Chakraborty S. Mahamuni C. V. Dharmadhikari P. Francis, S. Patil and S. V. Ghaisas. "Electronic and optical properties of agglomerated hydrogen terminated silicon nanoparticles". *Eur. Phys. J. D*, 67(144), 2003.

[63] W. G. Ding W. Yua, J. Y. Zhang and G. S. Fu. "Excitonic photoluminescence characteristics of amorphous silicon nanoparticles embedded in silicon nitride film". *Phys. J. B*, 57:53–56, 2007.

[64] A. Dong Q. Dong and Morigen. "Evaluation of Novel antimicrobial N-Halamine nanoparticles prodrugs towards susceptibility of *Escherichia coli* induced by DksA protein.". *Molecules*, 20:7292–7308, 2015.

[65] P. J. Launer. "Infrared analysis of organosilicon compounds : Spectra-structure correlations". *Laboratory for materials*, pages 100–103, 1987.

[66] P. G. Kale and C. S. Solanki. "Synthesis of Si nanoparticles from freestanding porous silicon (PS) film using ultrasonifucation". *PVSC*, pages 3692–3697, 2010.

[67] P. Gupta and M. Ramrakhiani. "Influence of the particle size on the optical properties of CdSe nanoparticles". *The Open Nanoscience Journal*.

[68] W. J. Lai Y. C. Yeh H. A. Chen I. S. Chen L. Chen K. H. Chen T. Nemoto S. Isoda M. Chen T. Fujita G. Eda H. Yamaguchi M. Chhowalla C. T. Chien, S. S. Li and C. W. Chen. "Tunable photoluminescence from graphene oxide". *Angew. Chem. Int.*, 51:6662–6666, 2012.

[69] T. Chang L. B. Can, P. X. Qin and W. Z. Long. "PLE spectra analysis of the sub-structure in the absorption spectra of CdSeS quantum dots". *Chin. Phy. Soc.*, 15(5):1067–1070, 2006.

[70] M. Kurtinatiene R. Juskenas A. Kareiva A. Beganskiene, V. Sirutkaitis. "FTIR, TEM and NMR investigations of Stober silica nanoparticles". *Materials science*, 10(4):287–290, 2004.

[71] P. Bankhead. "Analyzing fluorescence microscopy images with ImageJ". *Queens University Belfast*, 2014.

[72] University of Oxford Sir William Dunn, School of Pathology. "Applications of nanoparticles in biology and medicine". *Journal of Nanobiotechnology*, 2(3), 2004.

[73] C. Huan and S. S. Qing. "Silicon nanoparticles: Preparation, properties, and applications". *Chin. Phys. B*, 23:1–14, 2014.

[74] M. Nirmal and L. Brus. "Luminescence photophysics in semiconductor nanocrystals". *Acc. Chem. Res*, 32:407–414, 1999.

[75] M. M. Berekaa. "Nanotechnology in wastewater treatment; influence of nanomaterials on microbial systems". *Int.J.Curr.Microbiol.App.Sci*, 5(1):713–726, 2016.